



OPEN ACCESS

EDITED BY

Raghavan Chinnadurai, Mercer University, United States

REVIEWED BY

Wayne Robert Thomas, University of Western Australia, Australia Nicolas Bertho, INRA Biologie, Épidémiologie et Analyse de Risque en santé animale (BIOEPAR), France

*CORRESPONDENCE Stephanie C. Talker

[†]PRESENT ADDRESS

Gaël Auray,

Department of Biomedicine, University of Basel, Basel, Switzerland

[‡]These authors have contributed equally to this work

RECEIVED 02 June 2025 ACCEPTED 13 October 2025 PUBLISHED 29 October 2025

CITATION

Baillou A, Auray G, Brito F, Botos M, Huber A, Summerfield A and Talker SC (2025) Unraveling porcine dendritic-cell diversity: welcome tDC and DC3. Front. Immunol. 16:1639553. doi: 10.3389/fimmu.2025.1639553

COPYRIGHT

© 2025 Baillou, Auray, Brito, Botos, Huber, Summerfield and Talker. This is an open-access article distributed under the terms of the Creative Commons Attribution License (CC BY). The use, distribution or reproduction in other forums is permitted, provided the original author(s) and the copyright owner(s) are credited and that the original publication in this journal is cited, in accordance with accepted academic practice. No use, distribution or reproduction is permitted which does not comply with these terms.

Unraveling porcine dendritic-cell diversity: welcome tDC and DC3

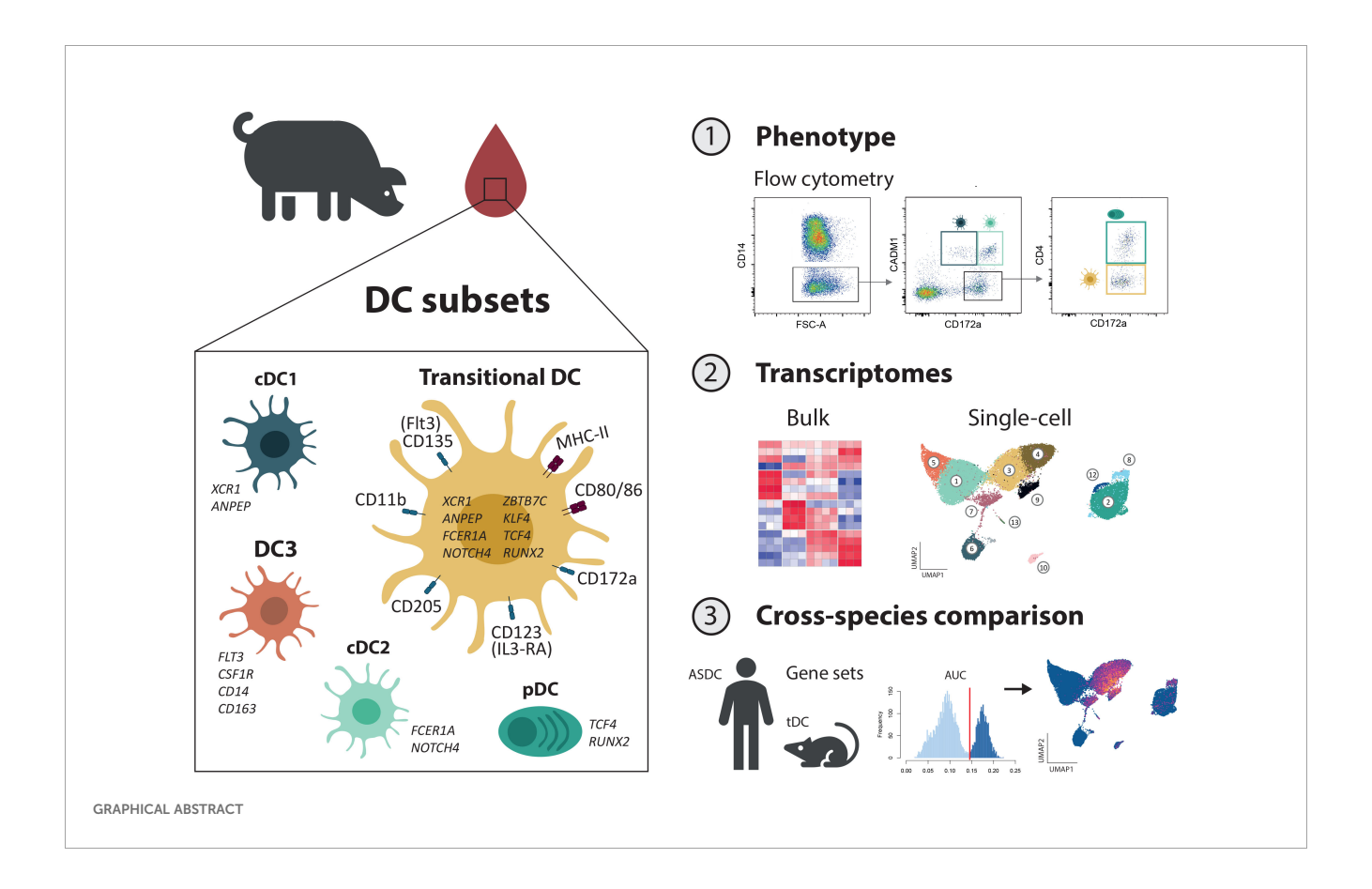
Ambre Baillou^{1,2}, Gaël Auray^{1,2†}, Francisco Brito^{1,2}, Marius Botos^{1,2}, Alizée Huber^{1,2}, Artur Summerfield^{1,2‡} and Stephanie C. Talker^{1,2*‡}

¹Institute of Virology and Immunology, Bern, Switzerland, ²Department of Infectious Diseases and Pathobiology, Vetsuisse Faculty, University of Bern, Bern, Switzerland

Dendritic cells (DC) are professional antigen presenting cells playing a major role in orchestrating adaptative immune responses. To adapt to various immune challenges, such as different classes of pathogens, specialized subsets of DC have evolved across species. To date, DC are classified as conventional DC (cDC1, cDC2) and plasmacytoid DC (pDC), with the more recent addition of DC3 and transitional DC (tDC) that were discovered in human and mouse thanks to high-dimensional phenotyping and single-cell sequencing technologies. Here, by combining flow cytometry and RNA-seq on the bulk- and single-cell level, we identified the porcine equivalent of tDC in blood as CD14⁻CADM1⁻CD172a⁺CD4⁻ cells expressing both Flt3 and CD123 (IL-3RA). This new subset forms a well-defined cluster when mapped onto scRNA-seq data of enriched DC and shares transcriptomic features and abundance with porcine blood cDC2 and pDC. Moreover, we describe putative porcine DC3 as transcriptionally overlapping cells in-between cDC2 and monocytes. With the core functions of tDC and DC3 remaining to be elucidated, our datasets provide a valuable resource for cross-species research on DC heterogeneity in various lymphoid and non-lymphoid tissues.

KEYWORDS

transitional dendritic cells, tDC, DC3, pig, blood, single-cell transcriptomics, bulk RNA-seq



Introduction

Dendritic cells (DC) are best known as instructors of T-cell immunity through antigen presentation and co-stimulation. Their response enables the system to adapt to various challenges and simultaneously ensures tolerance to harmless antigens. To fulfill these diverse roles, the DC system comprises phenotypically and functionally distinct cell subsets that have been extensively studied across tissues in humans (1, 2), mice (1, 3) and pigs (4, 5) among other species (6-10). Traditionally, DC have been broadly divided into two lineages: plasmacytoid DC (pDC), primarily known as IFN type 1 producers in response to viral infection, and conventional DC (cDC) which are highly efficient in stimulating T-cell responses. Conventional DC were further divided into type 1 cDC (cDC1) and type 2 cDC (cDC2), with cDC1 appearing specialized in the induction of Th1- and cytotoxic T-cell responses, and cDC2 preferentially promoting Th2/ Th17 responses (3). Subsets of cDC are broadly distributed across both lymphoid and non-lymphoid tissues and are also detectable in the circulation, with cDC2 more abundant than cDC1, particularly in mucosal and peripheral tissues. In contrast, pDC are rare in peripheral tissues and primarily localized in lymphoid organs and blood.

Over the last decade, high-dimensional and high-throughput approaches, such as single-cell RNA sequencing (scRNA-seq) (1), have revealed an astonishing heterogeneity and plasticity of cDC2 (1, 11, 12), with cDC2 subsets likely arising from distinct ontogenetic lineages (13–15) and being shaped by signals in their microenvironment (16). Moreover, highly pro-inflammatory cDC2

have been identified as a separate DC lineage, namely type 3 DC (DC3), overlapping with monocytes both phenotypically and transcriptionally and putting traditional monocyte markers like CD14 into question (12, 14, 17, 18).

Furthermore, the phenotypic definition of pDC was challenged, when putative pre-DC were discovered with scRNA-seq in humans and mice and shown to contaminate traditional pDC gates (19-21). Indeed, these putative pre-DC, shown to derive from pro-pDC and now classified as transitional DC (tDC), appear to be competent antigen presenters that have likely biased several in vitro assays involving pDC, as discussed elsewhere (19, 20, 22, 23). A murine coronavirus infection model has suggested the involvement of tDC in viral responses, with the intriguing hypothesis that tDC are in a delicate balance with antiviral pDC and enhance pro-inflammatory responses by IL-1β production (24). Notably, cDC2-like cells were shown to differentiate from tDC, and may be termed tDC2 as suggested by Sulczewski et al. (24). These tDC2 very much resemble ESAM+ cDC2 and CD5+ cDC2 in mouse and human, respectively, and were shown to replenish the DC2 pool in mouse models with impaired pre-DC2 development (24-26). This further complicates the picture of DC2 heterogeneity, now encompassing pre-cDC-derived cDC2 subsets (15), pro-DC3-derived DC3 (monocyte-like) (18), and pro-pDC-derived tDC2 (pDC-like) (24).

We have previously described phenotype and bulk transcriptome of porcine blood cDC1, cDC2 and pDC, with key gene expression confirming a gating strategy based on CD14, CD172a, CADM1 and CD4 (4). Accordingly, porcine cDC1 can be identified as CD14

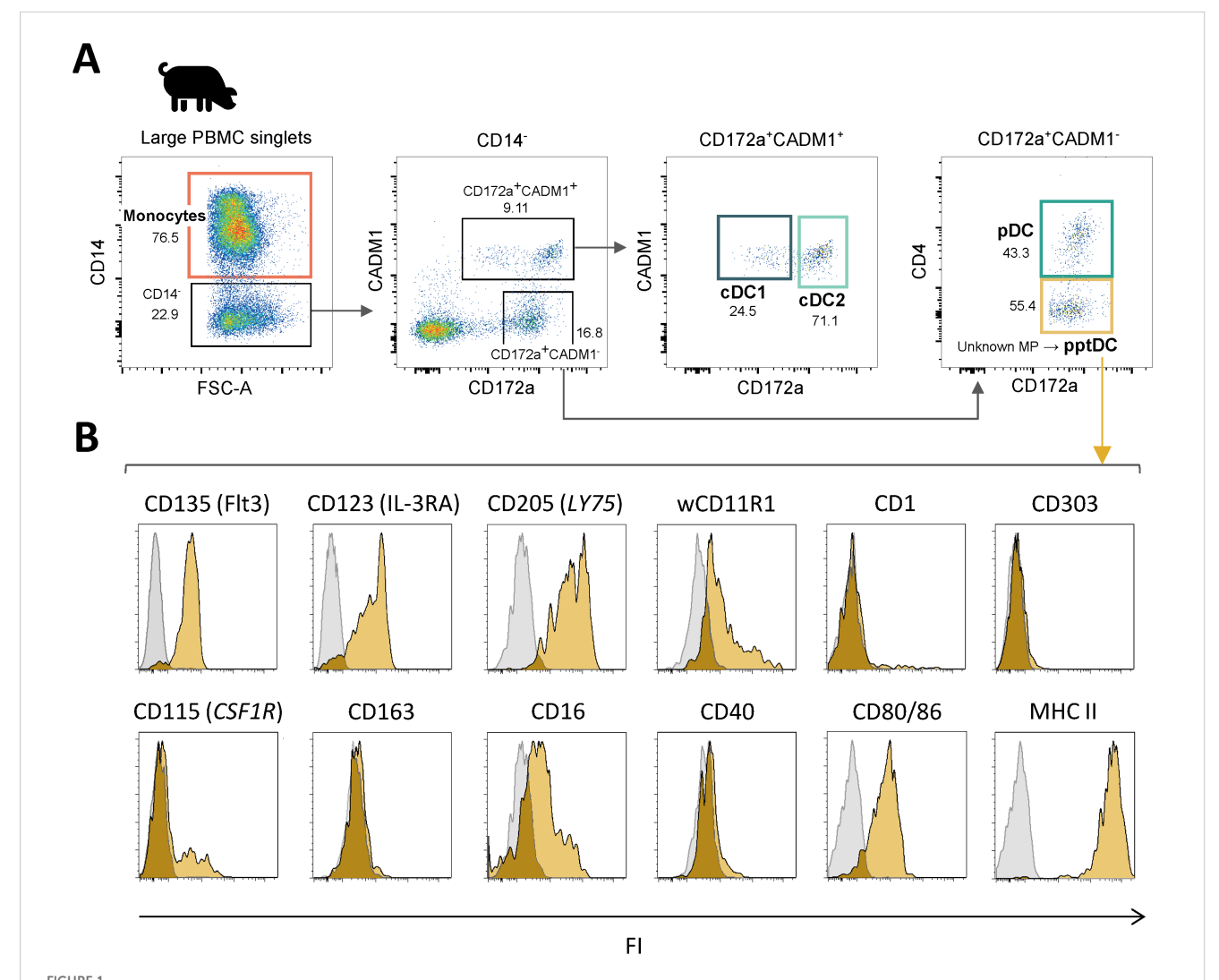
CD172a^{low}CADM1⁺CD4⁻, cDC2 as CD14⁻CD172a⁺CADM1⁺CD4⁻, and pDC as CD14⁻CD172a⁺CADM1⁻CD4⁺. Notably, using this marker combination, one additional subset was apparent, expressing CD172a, but lacking expression of all other markers (CD14⁻CADM1⁻CD172a⁺CD4⁻). By performing scRNA-seq on Flt3⁺ DC enriched from porcine blood, we now confirm the existence of this novel subset and identify it as porcine tDC. Moreover, we describe putative DC3 as cells co-expressing both cDC2 markers (*FLT3*, *FCER1A*, *CD1.1*) and monocyte markers (*CSF1R*, *CD14*, *CD163*, *C5AR1*).

Results

Phenotype of putative porcine tDC

In a previous study, we characterized mononuclear phagocyte (MP) subsets in porcine blood by flow cytometry, identifying cDC1

as CD14⁻CD172a^{low}CADM1⁺, cDC2 as CD14⁻CD172a⁺CADM1⁺, pDC as CD14⁻CD172a⁺CADM1⁻CD4⁺ and monocytes as CD14⁺ (4). Here, applying the same staining protocol and gating strategy (Supplementary Figure S1), we focused our analysis on the previously undescribed MP subset of CD14 CD172a cells lacking both CADM1 and CD4 expression and being as frequent as pDC in blood of pigs (Figure 1A). Expression of the conserved DC marker Flt3 (CD135), together with the almost complete lack of monocyte markers (CD115/CSF1R and CD163), supported its identification as a bona fide DC subset (Figure 1B). Notably, it shared phenotypic markers with both cDC (CD11b/wCD11R1 (27) and CD205, absence of CD303) and pDC (IL3-RA/CD123, absence of CD1). Moreover, this subset expressed CD80/86 and a high level of MHC-II, thus suggesting its involvement in antigen presentation and Tcell co-stimulation. Taken together, this new DC subset displayed a phenotypic profile overlapping with both cDC and pDC phenotypes, and it shared prominent expression of IL3-RA with



Phenotypic characterization of a new DC subset in blood of pigs: putative porcine tDC (pptDC). PBMC were isolated from the blood of four pigs and stained for flow cytometry. (A) Representative gating for mononuclear phagocyte (MP) subsets. Following selection of large cells and doublet exclusion (see Supplementary Figure S1), CD14⁺ cells were defined as monocytes and four subsets were distinguished among CD14⁻ cells: cDC1 as CD172a^{low}CADM1⁺, cDC2 as CD172a⁺CADM1⁺, pDC as CD172a⁺CADM1⁻CD4⁺, and a newly described DC subset as CD172a⁺CADM1⁻CD4⁻. (B) Yellow histograms show the expression of various molecules on CD172a⁺CADM1⁻CD4⁻ cells. Gray histograms show the FMO control.

pDC, leading us to further address this subset as putative porcine tDC (pptDC).

Bulk transcriptome confirms identity of putative porcine tDC

Following phenotypic characterization, we investigated the transcriptional profile of the newly identified pptDC. To this end, this subset was MACS/FACS-sorted from the blood of four pigs and processed for bulk RNA-seq. Resulting data were analyzed alongside previously generated RNA-seq datasets of the four other blood MP subsets (cDC1, cDC2, pDC and monocytes) (4). Principal component analysis (PCA) of the 500 most variable genes between the five MP subsets (PC1 = 60%, PC2 = 30%) showed that all samples of the newly described cell subset (pptDC) were clustering together and away from the four other MP subsets, supporting the discovery of pptDC as a new and distinct DC subset (Figure 2A). As further illustrated by a subset-to-subset correlation analysis, pptDC appeared to be more closely related to cDC than to pDC, sharing the highest correlation score with cDC2 (Supplementary Figure S2A).

Overall, gene expression was in line with surface protein expression detected in flow cytometry (Figure 2B). Gene expression for additional phenotypic markers is shown in Supplementary Figure S2B. Both pptDC and pDC expressed *IL3RA* (not available in Ensembl pig genome annotation), as shown by read mapping to the corresponding genomic region (Supplementary Figure S2C).

To characterize pptDC, we next studied the expression of conserved key genes known to define the main MP subsets across species (28, 29), including those we previously reported in pig blood (4). The updated analysis of the cDC1, cDC2, pDC and monocyte data (new reference genome) was in accordance with our formerly published transcriptomic analysis (4), supported also by the subsetspecific expression pattern of these markers (Figure 2C). For pptDC, the expression of the pan-DC markers FLT3 and BCL11A was in common with cDC1, cDC2 and pDC. Considerable levels of monocyte-specific gene expression (e.g. CSF1R, CD14, CD163) were detected in two out of four pptDC samples (#4, #5 in Figure 2C). Notably, pptDC expressed transcripts for both IRF4 and IRF8, two transcription factors (TF) involved in the development of cDC2 and cDC1/pDC, respectively (3, 28). In addition to markers shared across DC populations, pptDC showed expression of DC subsetrestricted features, such as XCR1 and ANPEP (cDC1), FCER1A, CD207 and NOTCH4 (cDC2), and RUNX2, TCF4, BLNK and SPIB (pDC).

Dendritic cells with a phenotype and transcriptome overlapping with both cDC2 and pDC are characteristic of the recently identified tDC in humans (19) and mice (22). These tDC were reported to originate from progenitors shared with pDC and to differentiate into cDC2 (24). To further explore if our new DC subset represents the porcine equivalent of tDC, we analyzed differentially expressed genes (DEGs) between pptDC and cDC2 or pDC based on pairwise comparisons (DESeq2). Complete lists of DEGs are provided as

Data S1. Putative porcine tDC showed expression of SPI1, TCF4, NOTCH2, CEPBA, KLF3, KLF8, KLF12, ZBTB46, IRF4, IRF8, STAT5A, RUNX2 and SPIB (Figures 2C, D), which are genes also found in tDC of humans and mice (22, 24, 30, 31), coding for cDCor pDC-specific transcription factors (TF). Notably, Leylek et al. demonstrated by chromatin accessibility analysis that KLF3, KLF8 and KLF12 were part of the unique TF profile of tDC (30). Among the gene regulatory network governing DC development, TCF4 and ID2 are reported as mutual functional antagonists promoting pDC versus cDC differentiation, respectively (32). We found that both were expressed in pptDC (Figure 2D), reinforcing their intermediate nature between cDC2 and pDC. Additionally, this new subset exhibited a high transcription level of ZBTB16, the gene encoding PLZF, a TF known to induce ID2 expression (33). Interestingly, pptDC shared the expression of KLF4 with cDC2, reported to be required for the differentiation of murine circulating pDC-like cells (identified as pre-DC2) into a subset of cDC2 (26). Unlike pDC, pptDC showed low IRF7 gene expression, suggesting its limited capacity to produce type I IFN, also distinguishing tDC from pDC in human and mouse (22). Moreover, its high transcription level of CD200R1, STAT5A and RAB3IL1 in comparison to cDC2 and pDC is consistent with the spleen tDC signature described by Sulczewski et al. in mice (24).

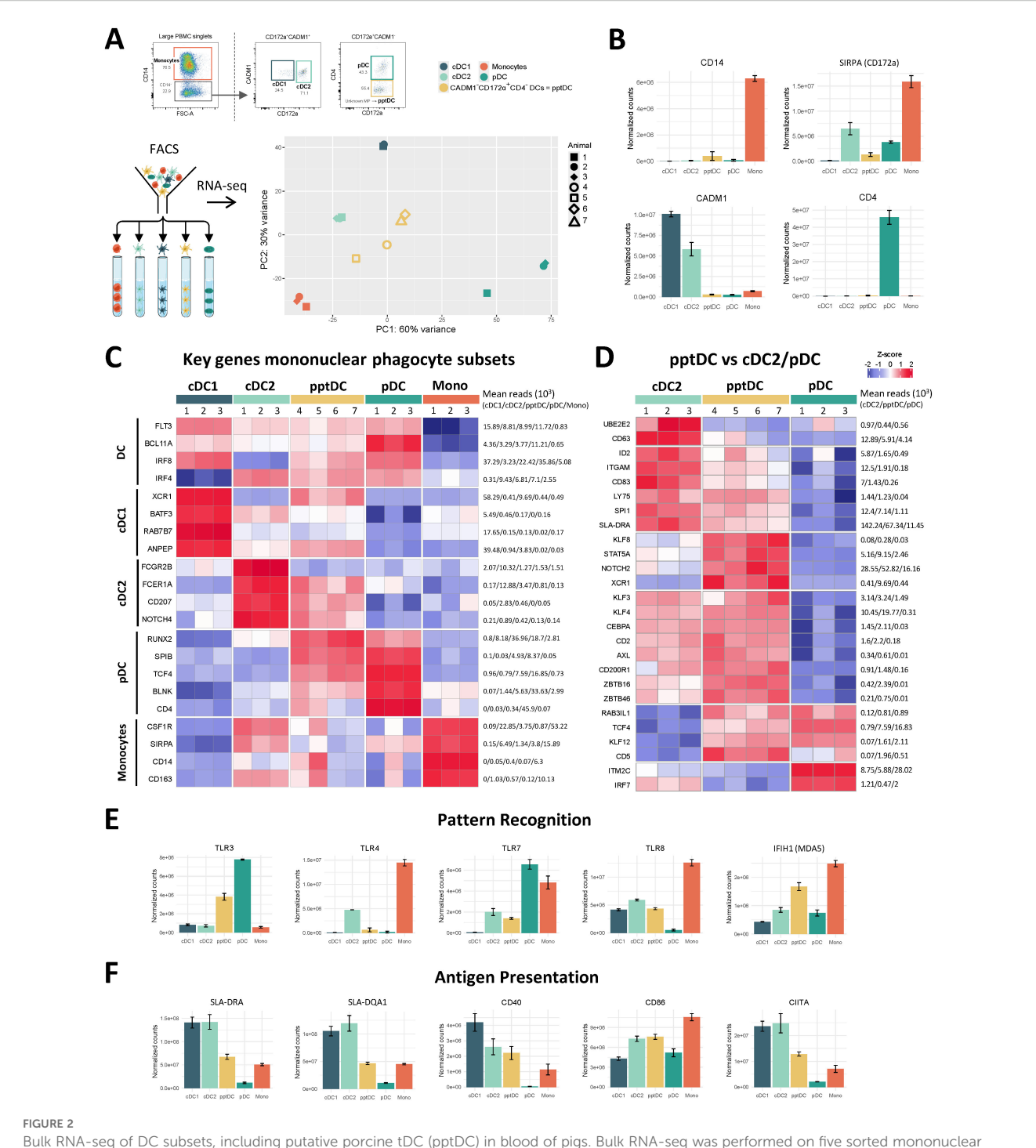
Porcine cDC2 and pptDC could be further distinguished from pDC by their expression of *AXL*, a human tDC marker (Figure 2D). Notably, pptDC expressed high levels of both *CD2* and *CD5*, in contrast to porcine pDC (low levels of *CD2* and *CD5* transcripts) and cDC2 (transcription of *CD2* but very low levels of *CD5* transcripts). These expression patterns were also found for human tDC, cDC2 and pDC, both transcriptionally and phenotypically (22). Thus, staining of CD2 and CD5 may be useful for distinction of porcine DC subsets in flow cytometry.

Finally, we observed a progressive increase of *ITGAM*, *CD83*, *LY75*, and *SLA-DRA* expression from pDC via pptDC toward cDC2 (Figure 2D), suggesting gradually increasing antigen presentation capabilities across those subsets. Taken together, phenotype and bulk transcriptomic signatures support the idea that the new porcine DC subset (CD14⁻CADM1 CD172a⁺CD4⁻) represents the equivalent of tDC described in human and mouse.

Functional specialization of pptDC inferred from bulk transcriptomics

Further exploration of pptDC-derived transcriptomic data revealed a unique gene signature related to pathogen recognition, antigen presentation, T-cell co-stimulation, immunoregulatory activities and cell adhesion (Figure 2 and Supplementary Figure S3).

Porcine putative tDC expressed relatively low levels of pattern recognition receptors (PPR) for bacterial components (e.g. *TLR4*, *TLR5*) (Supplementary Figure S3A), however one pptDC sample (#5) contained high transcript levels for bacterial PRR (Supplementary Figure S3A), and as shown in Figure 2C, also appeared enriched for monocyte-related transcripts such as *CD14*. Notably, all four pptDC samples stood out by high *TLR3* and *IFIH1*



Bulk RNA-seq of DC subsets, including putative porcine tDC (pptDC) in blood of pigs. Bulk RNA-seq was performed on five sorted mononuclear phagocyte (MP) subsets. (A) First two dimensions of principal component analysis, with different symbols representing individual animals. (B) Gene expression for markers used in FACS. Bar plots show the number of normalized counts for each gene and MP subset (mean ± standard deviation). (C) Transcription of key MP subset-defining genes represented by heatmap. Z-scores were calculated from log10-transformed normalized counts of selected genes. Mean kilo reads for each subset and gene are given to the right of each heatmap. (D) Gene transcription distinguishing putative porcine tDC (pptDC) from cDC2 and/or pDC. Genes were selected based on pairwise comparisons with DESeq2 (adjusted p-value < 0.05 and | log2FC| > 1) (see Data S1) and literature research. (E, F) Gene transcription for pattern recognition and antigen presentation. Bar plots show the number of normalized counts for each gene and MP subset (mean ± standard deviation).

(*MDA-5*) expression (Figure 2E), suggesting a specialization in sensing double stranded RNA. Transcripts for *TLR7*, *TLR8* and *TLR9* could also be detected in pptDC, even though higher levels were detected in other DC subsets.

Similar to cDC2, pptDC expressed a relatively high level of C-type lectin receptor (CLR)-associated genes, such as *MRC1* (*CD206*), *PLA2R1* (*CLEC13C*), *CD207* and *CLEC4F* (Supplementary Figure S3A), suggesting their involvement in mannose-ligand recognition

and phagocytic activities (34). Notably, expression of *MRC1* and *CLEC4F* was found to be very heterogeneous across pptDC samples. Similar to cDC1 and pDC, pptDC also contained transcripts for CLEC12A (MICL) and CLEC12B, two CLR that mostly recognize endogenous ligands such as damage-associated molecular patterns (35, 36), thus suggesting a role in clearing dying cells.

Looking at gene expression related to antigen presentation and T-cell modulation (Supplementary Figure S3B), pptDC stood out by expressing the highest levels of certain genes that may promote Tcell activation by enhancing antigen (cross-) presentation (ATG5, UBE2D1, RAB27A) (37-39), may promote the differentiation of regulatory T cells (IL4I1) (40, 41) or Th1 cells (DPP4) (42), or may otherwise be involved in regulating T-cell responses (VSIG10, CD200) (43, 44). For other genes involved in antigen presentation, we observed a gradual increase from pDC via pptDC towards cDC. Indeed, pptDC displayed intermediate transcription levels of genes encoding MHC-II molecules (e.g. SLA-DRA, SLA-DOA, SLA-DMB, SLA-DMA), molecules involved in MHC-II trafficking and antigen processing (PIKFYVE, IFI30, CIITA, CD74, LY75, TAP2) and co-stimulatory molecules (CD83, CD40) (Figure 2F, Supplementary Figure S2B, Supplementary Figure S3B).

Genes encoding cytokines and cytokine receptors predominantly expressed in pptDC included *IL18* and *IL17RA* (Supplementary Figure S3C). Notably, alongside cDC1, pptDC prominently expressed the beta chain of the IL-6 receptor (IL6ST), reported to function in signal transduction for various cytokines (45). When compared to pDC, pptDC contained fewer

across all clusters

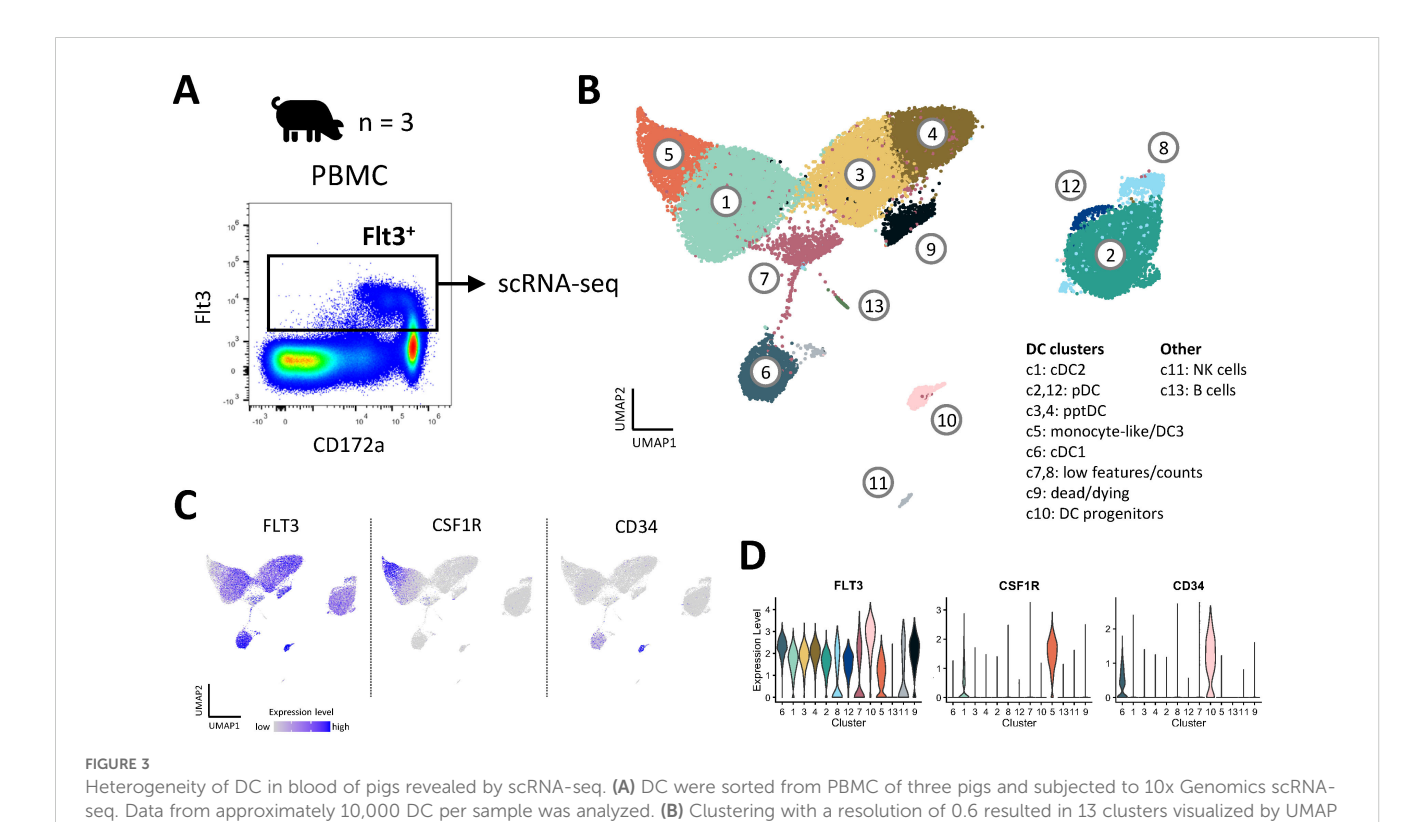
transcripts for type I interferons (*IFN-OMEGA-6*) and related receptors (*IFNAR1* and *IFNAR2*), reinforcing the hypothesis of their limited involvement in type I IFN responses.

Looking at chemokines and chemokine receptors, pptDC were found to express considerable levels of *XCR1* (Supplementary Figure S3D). Notably, this key marker for cDC1 is involved in antigen cross-presentation and CD8⁺ T-cell priming (46, 47). Moreover, pptDC contained the highest number of *CCR7* and *CXCR5* transcripts among cDC subsets, however at low levels (mean reads of 200 and 300, respectively). While CCR7 is a well-known marker for DC activation (48), expression of CXCR5 is expected to cause migration to the CXCL13-rich parafollicular areas of the lymph node to possibly stimulate follicular Th cells (49).

Finally, several genes encoding integrin chains showed highest expression in pptDC such as *ITGB3*, *ITGAV* and *ITGA6* (Supplementary Figure S3E), as well as genes encoding Fc receptors (e.g. *FCRL4*) (Supplementary Figure S3F), metalloproteinases (e.g. *MME* and *MMP9*) (Supplementary Figure S3G) and semaphorins (e.g. *SEMA4F*, *SEMA4C*, *PLXNA4*) (Supplementary Figure S3H).

Heterogeneity of porcine blood DC revealed by scRNA-seq

To get a more unbiased view on the heterogeneity of porcine blood DC subsets, we performed scRNA-seq (10x Genomics) on Flt3⁺ DC enriched from blood of three pigs (Figure 3A). Clustering of cells with a resolution of 0.6 (Leiden algorithm) resulted in the



plot. (C) Feature plots showing the expression of FLT3, CSF1R and CD34. (D) Violin plots showing the level of FLT3, CSF1R and CD34 expression

identification of thirteen distinct clusters (Figure 3B). Complete lists of cluster-defining marker genes, as determined by Seurat's *FindAllMarkers()* function, are listed in Data S3. Three clusters (c7, c8, c9) were excluded due to quality issues (Supplementary Figure S4A), as were clusters containing B cells (c13) and NK cells (c11) (Supplementary Figures S4B, S4C).

Eight FLT3-expressing clusters (c1, c2, c3, c4, c5, c6, c10, and c12) were analyzed in further detail. Notably, cluster 5 appeared to contain monocytic cells alongside DC (DEG including CSF1R, C5AR1, CD14, CD163, SIRPA and CD68), and cluster 10 appeared to be comprised of DC progenitors (DEG including CD34, MEIS1, DACH1, ERG, KIT, IKZF2 and MECOM) (15) (Figures 3C, D, Data S3). As shown in Figures 4A–C, expression of subset-specific key genes clearly identified cluster 6 as cDC1 (BATF3, XCR1, RAB7B, ANPEP, IRF8), cluster 1 as cDC2 (FCER1A, FCGR2B, CD207, SIRPA, IRF4) and clusters 2 and 12 as pDC (CD4, SPIB, BLNK, TCF4, RUNX2, IRF8). Cells in clusters 3 and 4 expressed IRF4, IRF8, XCR1, ANPEP, FCER1A, RUNX2, SPIB, TCF4 and BLNK (Figure 4B), thus sharing subset-specific markers with cDC1, cDC2 and pDC, as observed with bulk RNA-seq of pptDC described above (Figure 2C).

A heatmap of the top 15 (adjusted p-value) DEG between the DC subsets is shown in Figure 4C and the complete gene lists are given in Data S3. Apart from the genes mentioned above, DEG included CADM1, CLNK, ID2, SNX22, WDFY4 and DNASEIL3, for cDC1 (c6), CD1D, ITGAM (CD11b), S100A4, TLR2 and TLR4 for cDC2 (c1), and IRF7, IFNAR1, NRP1, LRP8 and SYK for pDC (c2, c12). In line with the bulk RNA-seq analysis (Figure 2, Data S1), clusters 3 and 4 were enriched for ZBTB7C, ZBTB16, KLF4, NOTCH2, DPP4 (CD26), TGFBR3 and SEMA4F, further supporting the classification of c3 and c4 as pptDC.

Correlation of FCM-based and scRNA-seq based subset identification

When estimating the proportions of the DC clusters within total blood DC (Figure 4D), we found that c1 (cDC2) and c2 (pDC) each represented approximately 30%, c6 (cDC1) represented 7%, and the pptDC clusters 3 and 4 represented 16% and 14%, respectively. These results are in accordance with the cell proportions previously observed by flow cytometry for the RNA-seq analysis of sorted cells (Figure 1A). Representative flow cytometry data for animals included in the scRNA-seq analysis is shown in Supplementary Figure S5. Proportions of DC subsets from scRNA-seq and flow cytometry showed a moderate correlation, with an R² value of 0.65 (Figure 4E).

To investigate if flow-cytometry defined DC subsets are well represented in the clustering of the scRNA-seq dataset, we tested for relative enrichment of the gene signatures from sorted bulk-sequenced subsets in the scRNA-seq clusters by gene-set enrichment analysis (GSEA). Different levels of enrichment were tested (5, 10, 15, 25, 50 and 100%) (see Material and Methods), allowing us to select 25% for optimal resolution of sc identities (Supplementary Figure S6). As shown in UMAP plots (Figure 4F)

and a heatmap (Figure 4G), cDC1-derived gene sets had the highest enrichment in cluster 6, cDC2-derived gene sets in cluster 1, pDC-derived gene sets in clusters 2 and 12, and pptDC-derived gene sets in clusters 3 and 4. This clear allocation of bulk signatures supports the suitability of the 4-marker sorting strategy for porcine DC subsets and confirms the cluster identification in the scRNA-seq dataset.

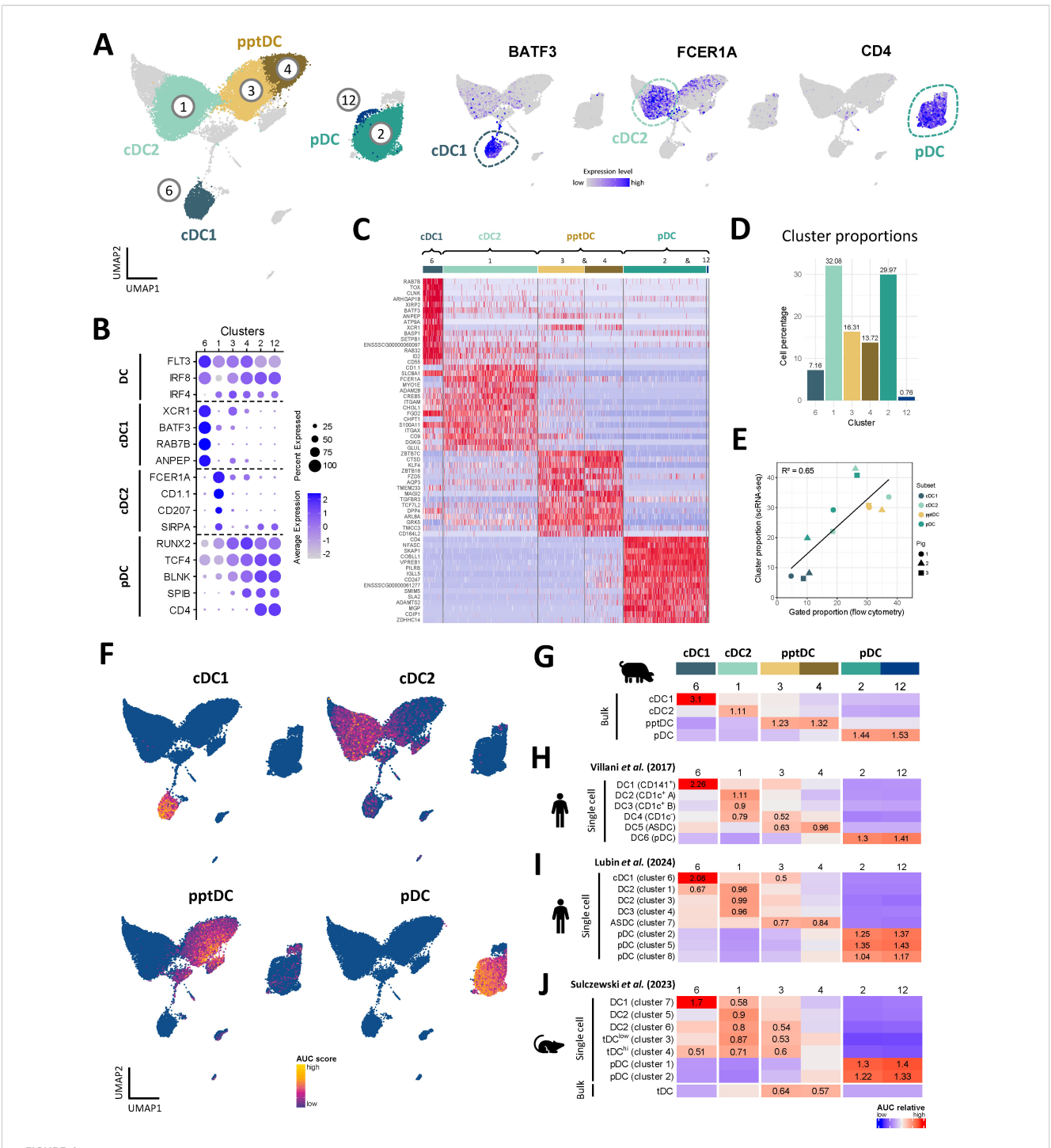
Putative porcine tDC share transcript signature with human and murine tDC

For further verification of pptDC identity, we used the GSEA approach described above to compare the porcine DC signatures to DC signatures derived from published bulk- and scRNA-seq studies of human blood (19, 50) and murine spleen (24) (Figures 4H–J). Two distinct human studies were selected, each utilizing a different scRNA-seq technology (SMARTSeq2 for Villani et al. (19), Figure 4H, and 10x Genomics for Lubin et al. (50), Figure 4I and Supplementary Figure S7). As expected, both human and murine cDC1, cDC2 and pDC gene signatures showed the highest relative enrichment in cluster 6 (cDC1), cluster 1 (cDC2) and in clusters 2 and 12 (both pDC), respectively. Notably, human ASDC and murine tDC ("bulk") gene sets showed the highest enrichment in clusters 3 and 4, representing pptDC (Figures 4H–J), thus supporting the identification of pptDC as porcine equivalents of tDC.

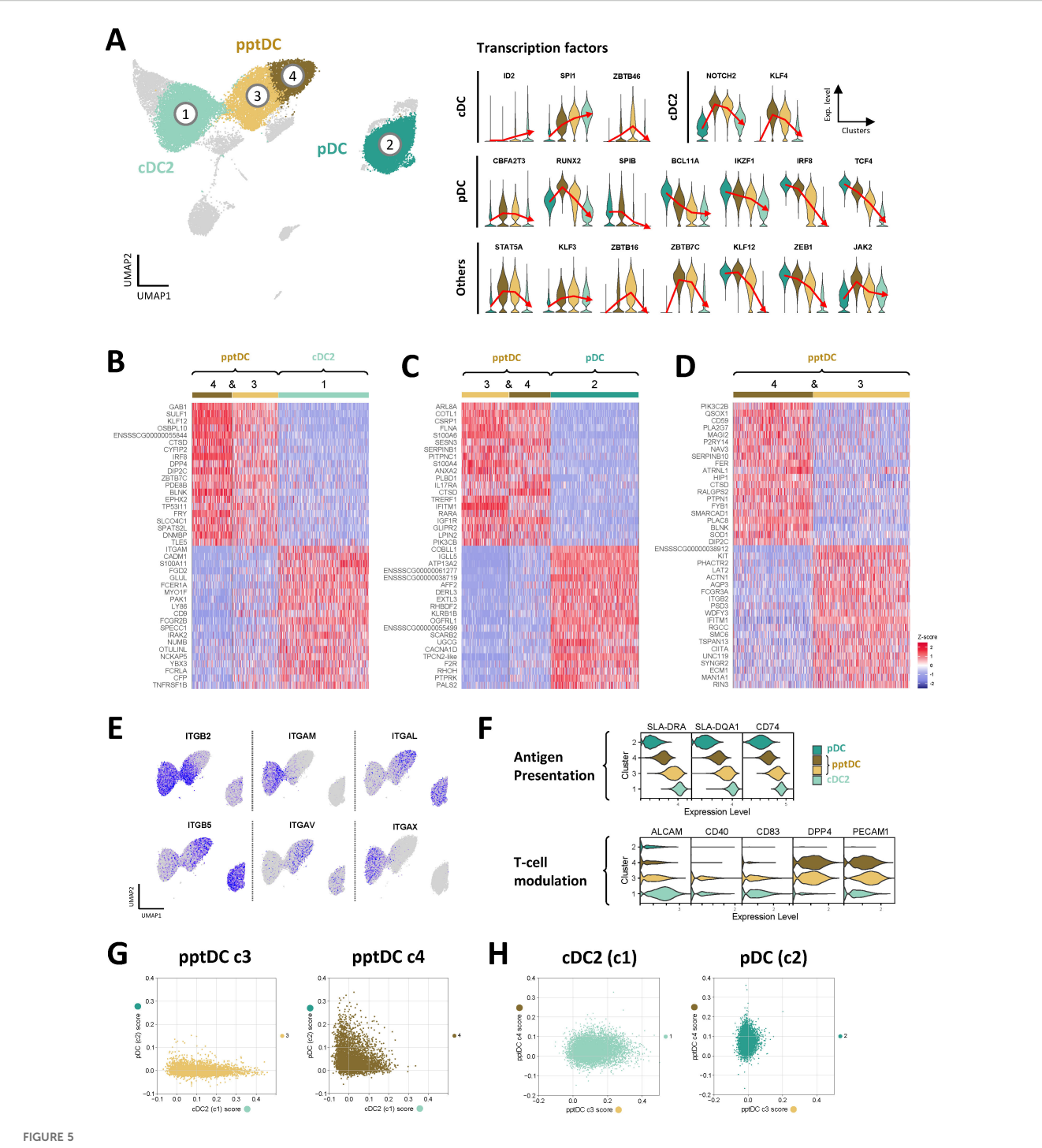
As expected, cluster 4 (pDC-like pptDC) was more enriched for human and murine pDC signatures than cluster 3 (cDC2-like pptDC), whereas cluster 3 displayed greater enrichment for human and murine cDC2 signatures than cluster 4. However, sc signatures of murine tDC-subclusters ("tDClow" and "tDChi") did not show discriminating enrichment in pptDC clusters 3 or 4 (Figure 4J) but were rather enriched in c3 (cDC2-like pptDC) and c1 (cDC2).

pptDC span a continuum between pDC-like and cDC-like profiles

In accordance with the reported origin of tDC from pro-pDC and their differentiation into cDC2-like cells (14, 15, 24, 26, 50), we found that transcripts for several TF involved in DC fate decisions (28) were sequentially increased or decreased from pDC via pptDC (c4 and c3) towards cDC2 (Figure 5A). Among TF, the most evident gradual decrease was observed for pDC-associated genes *TCF4*, *IRF8*, *IKZF1* and *BCL11A*, whereas transcription of cDC-associated genes *SPI1* and *ID2* increased via c4 and c3. A more abrupt decrease from c4 to c3 was observed for *SPIB*, the gene coding for Spi-B, a transcription factor promoting development of pDC (51). Notably, *RUNX2*, *NOTCH2*, *KLF4*, *KLF12* and *JAK2* showed highest expression in c4, before decreasing again in c3, whereas *ZBTB46* and *ZBTB16* expression appeared to peak in c3. Lastly, several TF showed increased expression in both c3 and c4 when compared to pDC and cDC2 (*ZBTB7C*, *STAT5A*, *KLF3* and *CBFA2T3*).



Annotation of DC subsets, including pptDC, in scRNA-seq dataset. (A) Subset annotation of main DC subsets (left) and expression of key genes visualized in feature plots (right). (B) Dot plot showing DC-subset-defining key genes. (C) Heatmap showing the top 15 differentially expressed genes (p_val_adj) for main DC clusters, as determined by Seurat's FindAllMarkers() function. Complete gene lists are available as Data S3. (D) Proportion of each DC cluster relative to the total selected DC population. (E) Correlation between cell proportions obtained from scRNA-seq (y-axis) and flow cytometry (x-axis) of the same pigs. Symbols represent individual animals. Black line represents the linear regression model. (F) Enrichment of gene signatures from bulk-sequenced DC subsets (see Data S1) in single-cell RNA-seq clusters represented by UMAP plots. (G—J) Heatmaps showing averaged scaled enrichment scores for gene signatures from bulk-sequenced porcine DC subsets (see Data S1) (G), from human blood DC (Villani et al.) (H), from re-analyzed human blood DC (Lubin et al., for re-analysis see Supplementary Figure S7) (I), and from murine spleen DC (Sulczewski et al.) (J) (see Data S2). AUC relative scores >= 0.5 are displayed.



Transcriptomic delineation of pptDC from pDC and cDC2. Comparison of cDC2 (c1), pDC (focus on c2) and pptDC clusters (c3 and c4). (A) Violin plots show gene expression for transcription factors involved in the development of different DC subsets. Red lines pass through the mean expression value for each cluster. (B-D) Heatmaps show the top 20 differentially expressed genes (p_val_adj) in selected DC clusters, as determined by Seurat's FindMarkers() function for pairwise comparisons. Complete gene lists are available as Data S3. (E) Feature plots showing the expression of genes coding for different integrin chains. (F) Expression of genes related to antigen presentation and T-cell modulation. (G, H) Single-cell classification scoring determined with an ElasticNet model.

The transcriptomic signature of pptDC clusters (c3 & c4) was further characterized by comparing them against cDC2 (c1) and pDC (c2) and against each other. Heatmaps of the top 20 (adjusted p-value) DEGs are shown in Figures 5B–D. The complete gene lists are given in Data S3. Notably tDC clusters differed in the expression

of integrin transcripts (Figure 5E), generally reflecting their similarity to either pDC (c4: *ITGAL*, *ITGB5*) or cDC2 (c3: *ITGB2*, *ITGAM*, *ITGAX*). In accordance with the adoption of an increasingly cDC-like phenotype, cDC2-like tDC (c3) showed higher expression of transcripts related to antigen presentation

(e.g. SLA-DRA, SLA-DQA1, CD74) and T-cell stimulation (e.g. CD40, CD83, ALCAM) than pDC-like tDC (c4) (Figure 5F). In line with bulk RNA-seq, pptDC clusters showed the highest expression of DPP4 and PECAM1 (two genes involved in T-cell modulation), when compared to pDC and cDC2.

To further characterize the correlation between pptDC and cDC2 or pDC, we trained an ElasticNet model computing a classification score based on the transcriptomic signatures of the different cell types (Figures 5G, H). According to this model, pptDC in cluster 4 showed low-to-intermediate scores for both cDC2 and pDC signatures, while pptDC in cluster 3 were characterized by a progressive increase in the cDC2 score while exhibiting a low pDC score (Figure 5G). In line with the differential gene expression analysis, cDC2 displayed a higher score for cluster 3 than for cluster 4, and pDC showed the reverse pattern (Figure 5H).

Overall, the transcriptome of pptDC spans a continuum between pDC and cDC profiles, as described for humans and mice (19, 22, 24, 52). This intermediate transcriptome, together with the core gene signature resembling human and murine tDC, justifies identifying pptDC as the porcine equivalents of ASDC/tDC. Furthermore, these results suggest that porcine tDC may differentiate into cDC2-like cells, as proposed for their murine (24, 26) and human (50) counterparts.

To further explore the cellular dynamics between porcine tDC and cDC2, we performed a trajectory inference (TI) analysis on cells in clusters 1, 3 and 4 (Supplementary Figure S8). Genes that varied along the inferred trajectory corresponded to the DC subset-specific signatures previously identified by differential expression analysis. Notably, the continuum from tDC to cDC2 was marked by a gradual increase in the expression of genes associated with antigen presentation via MHC-II molecules (module 2 in Supplementary Figure S8C), suggesting a progressive acquisition of cDC features by tDC differentiating towards cDC2-like cells.

Putative DC3 in porcine blood

In both mouse and human, DC3 have been described as a novel DC subset sharing dendritic and monocytic markers (12, 14, 17–19). Interestingly, cluster 5, adjacent to cDC2 (c1), appeared to contain both monocytic and dendritic cells (Figure 3) and showed the highest enrichment score when performing GSEA with human DC3 signatures (Figures 6A, B).

Upon re-clustering of c5, two major clusters were separated from two smaller clusters (Figure 6C). The small clusters 3 and 4 were annotated as cDC2 (FLT3, FCER1A, CD1.1) and monocytes (high levels of CD14, LYZ), respectively, while the two major clusters 1 and 2 were annotated as putative DC3 as they contained low levels of CD14 and FCER1A transcripts alongside FLT3 and CSF1R transcripts (Figures 6C, D). Indeed, a significant proportion of cells in sub-clusters 1 and 2 (putative DC3) were revealed to co-express FLT3 transcripts alongside transcripts typically associated with monocytes, such as CSF1R, CD163, CD14 and C5AR1 (Figure 6E).

Among putative DC3, c1 stood out by higher transcription of *CD163*, *C5AR1* and *VCAN*, while c2 was clearly enriched in *S100A4*, *S100A6* and *CST3* transcripts (Figure 6F). Compared to c1, c2 also expressed slightly higher levels of MHC-II-related genes.

The current gating strategy for identifying porcine DC subsets is based on exclusion of CD14⁺ monocytes (Figure 1) and therefore likely excludes CD14-expressing DC3. This is illustrated by gradual gating based on CD14 expression prior to DC gates, as shown in Figure 6G. Indeed, CD14^{low} (P3) and CD14^{int} (P2) populations contained approximately 66% and 6% Flt3⁺ DC, respectively, mainly falling within the cDC2 gate (CADM1⁺CD172a⁺). The gated Flt3⁺CADM1⁺CD172a⁺ population thus represents a more heterogenous population, likely containing CD14-expressing DC3. This hypothesis is further supported by the shared expression of CADM1 and CD172a (*SIRPA*) by cDC2 (c1) and putative DC3 (c5) at the transcriptomic level (Figure 6H).

Discussion

We have previously identified porcine cDC1, cDC2 and pDC in blood of pigs by their expression of key transcripts conserved across species (4). In this previous work, we found a substantial subset of CD14⁻CADM1⁻CD172a⁺CD4⁻ cells in the blood of pig with unknown identity (4). Based on recent insights from human and mouse, the present study now identifies this unknown DC subset as the equivalent of tDC by combining flow cytometry, bulk- and scRNA-seq analyses.

With the current study, we have zoomed into the DC compartment by performing scRNA-seq on Flt3-enriched PBMC, revealing both tDC and putative DC3 in blood of pigs. Like their human and murine counterparts (19, 22, 24, 53), porcine tDC displayed a distinct transcriptomic signature in-between pDC and cDC2, whereas putative DC3 clustered in a continuum in-between cDC2 and monocytes.

Notably, porcine tDC were found to be as frequent as other DC subsets in blood of pigs, which is in stark contrast to reports from human and mouse, where tDC only form a minor population of approximately 1-5% among total DC in blood and spleen (19, 22, 24, 26, 50, 52). The high proportion of tDC in porcine blood is puzzling and may point towards high frequencies of tDC across tissues, which would make the pig an attractive model for studying tDC in various settings, including infection. In fact, tDC are discussed to play a special role in viral infection. In murine models of SARS-CoV2 infection, virus-sensing tDC produced IL-1 β and were deemed responsible for shifting the balance towards inflammation and fatal immunopathology (24). Upregulation of IL-1β was also observed in human tDC recruited to skin following experimental injection of UV-killed E. coli (50). Compared to blood tDC, these tDC had upregulated proinflammatory genes (IL1B, SAT1, AXL), genes related to IFN signaling (ISG15, IFI44L, IFI27), and chemokine receptors associated to migration (CXCR4, CX3CR1), while having downregulated genes coding for HLA molecules.

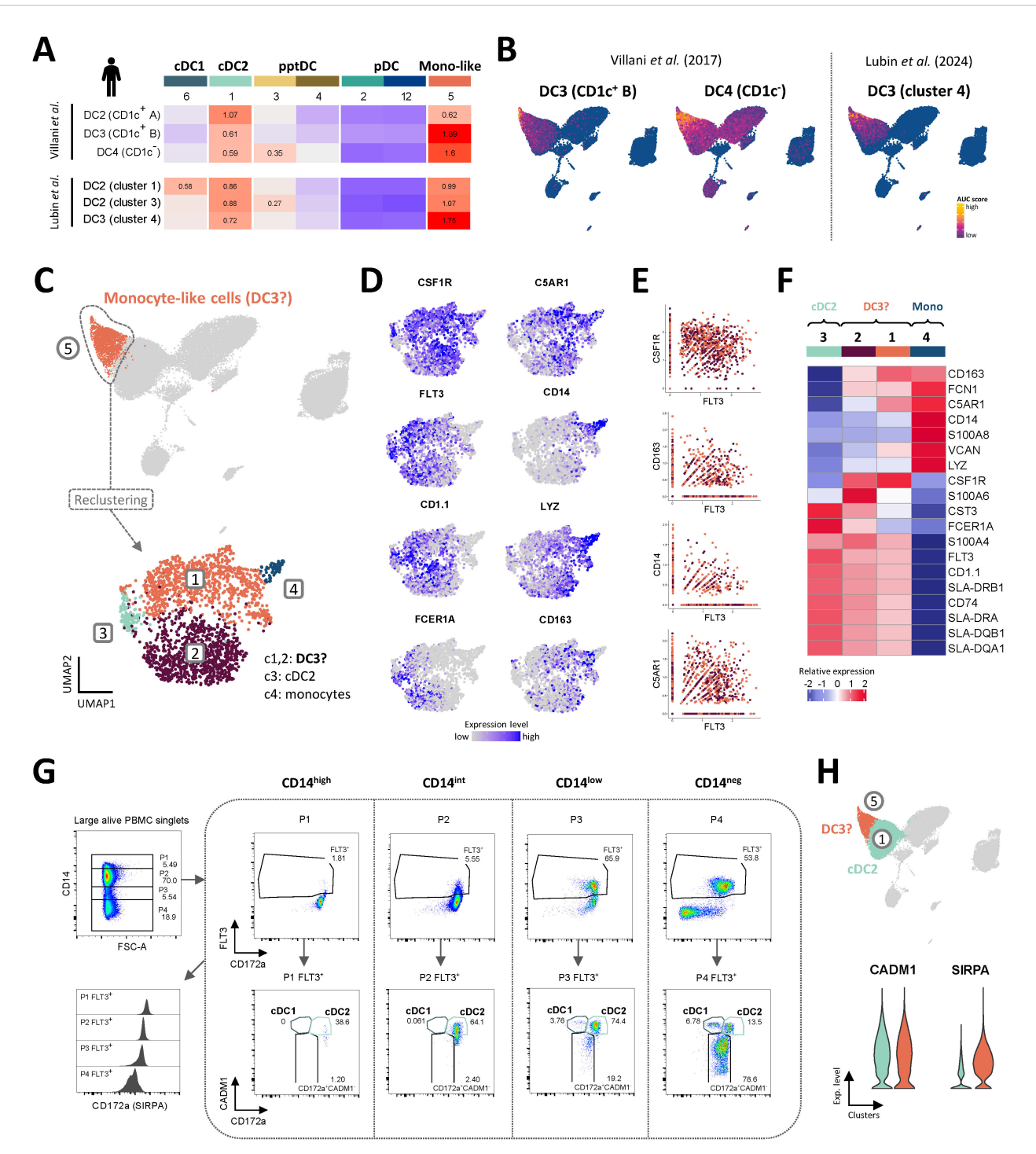


FIGURE 6

Putative porcine DC3 co-express FLT3 and CD14. (A, B) Enrichment of gene signatures from human blood DC2 and DC3 (Villani et al. and Lubin et al.), represented by heatmaps (A) and UMAP plots (B). AUC relative scores >= 0.5 are displayed. (C) Re-clustering of monocyte-like cells in cluster 5, resulting in 4 distinct clusters visualized by UMAP plot (Leiden algorithm, clustering resolution = 0.4). (D) Feature plots show expression of selected genes reported to distinguish human cDC2, DC3 and monocytes. (E) Scatter plots show co-expression of *FLT3* and selected monocytic markers in clusters 1 and 2. (F) Heatmap shows relative mean gene expression across each cluster for selected genes reported to distinguish between human cDC2, DC3 and monocytes. (G) Flow-cytometric gating of porcine DC subsets from gradual CD14 expression gates (P1-4). Plots are representative for all three pigs included in the scRNA-seq analysis. For complete gating strategy see Supplementary Figure S5. (H) Violin plots showing the expression of genes encoding CADM1 and CD172a (SIRPA) for the cDC2 (c1) and DC3 clusters (c5) in the original scRNA-seq dataset.

Our transcriptomic data support the involvement of porcine tDC in sensing viral components and in promoting inflammation. In particular, tDC might be involved in antiviral response by sensing double-stranded RNA via TLR3 expression. Notably, apart from porcine tDC, TLR3 is predominantly expressed in porcine pDC. This is in contrast to human and mouse, where TLR3 is not expressed at all on pDC (54, 55), representing only one example of species differences in viral sensing (4).

Porcine tDC expressed higher levels of CD86 and MHC-II molecules than pDC, both on the mRNA and protein level, suggesting that tDC are better equipped for T-cell stimulation. This is in line with murine and human tDC reported to outperform pDC in inducing allogenic T-cell proliferation (19, 22, 24, 26, 50). In fact, contaminations with tDC/human ASDC in traditional pDC gates have likely biased T-cell stimulation assays, erroneously attributing T-cell stimulatory functions to pDC (19). It remains to be determined if tDC contribute to stimulation of naive T cells in secondary lymphoid tissues. In a model of murine influenza infection, tDC were described to be recruited to the lungs, but were not found to accumulate in draining lymph nodes (22). While our data indicate transcription of several TLR and co-stimulatory molecules, future studies should interrogate TLR responsiveness and the capacity of porcine tDC for phenotypic maturation (upregulation of CCR7, MHC-II, CD80/86), as previously performed for bovine DC and monocyte subsets (8, 56). In particular, assessment of CCR7 upregulation upon TLR stimulation will indicate if porcine tDC are capable of migration to T-cell zones in secondary lymphoid tissues. The transcriptomic reference datasets generated in the present study will enable detailed investigations on tDC and their activation signatures across tissues both in steady-state and infection.

Murine studies have started to dissect the developmental pathway of tDC using specific knockout (KO) and adoptive cell transfer approaches, as well as lineage tracing mouse models (15, 24, 26). Sulczewski et al. demonstrated that murine tDC originate from bone marrow progenitors shared with pDC (pro-pDC) at steady state (24). Notably, when knocking out the pre-cDC pathway, pro-pDC could compensate for the lack of cDC2 by producing cDC2-like cells (termed tDC2) via the tDC pathway. Moreover, tDC isolated from human blood converted into CD5+ cDC2 upon CD40L stimulation in vitro (24) and bone marrow tDC cultured under standard DC differentiation conditions (i.e. GM-CSF and Flt3-ligand) generated exclusively DC2 (14). The clustering we observed in our scRNA-seq dataset alongside the transiently increasing cDC signature would support the hypothesis that porcine tDC can give rise to cDC2-like cells in vivo. It is intriguing to speculate that the bridge-like connection between cDC2-like tDC and cDC2 in our UMAP plot marks this transition. Recently, Lubin et al. used deuterium-glucose labeling of dividing cells to study the kinetics of DC subsets and their progenitors in human blood (50). Their findings support a model in which ASDC (human tDC) give rise to DC2 in both the bone marrow and blood. Indeed, the incorporation of deuterium into DNA is safe for use in humans and rodents (57, 58), making it a promising tool for investigating the fate and lifespan of DC in large animal models in vivo.

Patterns of expressed transcription factors in porcine tDC were largely in accordance with murine and human tDC. High expression of *STAT5A* in porcine tDC is in line with the idea that tDC need to counteract differentiation towards pDC, as STAT5 was reported to inhibit pDC development by suppressing IRF8 (59). By chromatin accessibility analysis, Leylek et al. demonstrated that KLF3, KLF8 and KLF12 were part of the unique TF profile of tDC (30). Accordingly, the distinct expression pattern of *KLF3*, *KLF8* and *KLF12* in porcine tDC distinguished them from cDC2 and pDC. Among the gene regulatory network governing DC development, TCF4 and ID2 are reported as mutual functional antagonists promoting pDC versus cDC differentiation, respectively (32). The expression of both *TCF4* and *ID2* in porcine tDC aligns with their transitional nature.

To our knowledge, tDC have not yet been described in mammalian species other than humans and mice. A decade ago, Vu Manh et al. described a subpopulation of cDC2 (FSC^{hi}MHC-II⁺CD14⁻CD4 CADM1⁻CD172a^{int}) in porcine blood (29). The bulk transcriptome of this population was suggested to be significantly contaminated by pDC (*TCF4*) and cDC1 (*XCR1*) and was thus excluded from their analyses. In the light of current knowledge and our present results, this population likely contained tDC. As did the *FLT3*- and *XCR1*-expressing CADM1⁻ population within CD14⁻ CD172a⁺CD1⁻CD4⁻ cDC reported in another study (60).

Transcriptomic data suggest that CD2 and CD5 can be used in flow cytometry to discriminate porcine tDC (CD2⁺CD5⁺) from pDC (CD2^{low}CD5^{low}) and cDC2 (CD2⁺CD5^{low}). Notably, human tDC, previously considered as pre-DC, are also reported to differ from pDC by expression of CD2 and CD5 transcripts (19, 53). Protein-level analyses are necessary to confirm the suitability of these markers.

The combination of bulk RNA-seq from sorted DC populations and scRNA-seq of enriched DC allowed us to confirm the accuracy of our flow-cytometry based subset identification (cDC1, cDC2, pDC, tDC). However, scRNA-seq of enriched DC revealed additional heterogeneity. Unbiased clustering of our scRNA-seq dataset suggests the presence of two tDC subsets in porcine blood, spanning a differentiation continuum in-between pDC-like cells and cDC2-like cells. Similarly, in mice, tDC were classified into two distinct subpopulations according to their similarity to pDC and cDC2, termed tDC^{low} (CD11c^{low}Ly6c^{high}) and tDC^{high} (CD11c^{high}Ly6C^{low}), respectively (22). The mouse Ly6c gene does not have a pig ortholog, but transcription of ITGAX, encoding CD11c, appeared to be higher in porcine cDC2-like tDC. So, although transcriptomic signatures from murine tDChigh and tDClow were not discriminatory for the two porcine tDC clusters, CD11c may still be suitable for distinguishing porcine tDC subsets in flow cytometry. Observed monocyte signatures (increased transcripts for e.g. CD14) in two out of four investigated tDC samples are surprising and cannot be explained by the scRNA-seq data, where monocyte-associated gene expression could not be detected in the two tDC clusters.

In addition to tDC, our scRNA-seq analyses suggest the presence of DC3 in porcine blood. Dendritic cells type 3 have been described as a new DC lineage, originating from monocyte/dendritic-cell precursors, as opposed to cDC deriving from common dendritic progenitors (15, 18). As DC3 share phenotype and transcriptome

with monocytes and cDC2, their clear delineation has proven difficult in both human and mouse, especially under inflammatory conditions (61). In fact, CD14, a molecule that has traditionally been used as a monocyte marker across species, appears to be expressed on DC3 of all species investigated so far, including pig. Notably, in the gating strategy employed here to sort porcine DC subsets for bulk RNA-seq, CD14+ cells were excluded. This has likely reduced DC3 contamination in the cDC2 gate, but also highlights the importance of scRNA-seq as a tool that is relatively independent of *a priori* defined gating strategies. In future studies, the gating strategy for porcine DC subsets should include Flt3 to account for CD14-expressing DC3.

When studying rare and poorly defined DC with scRNA-seq, proper enrichment strategies are crucial and should be based on extensive phenotypic characterization to not bias investigations on DC heterogeneity. By enriching DC by Flt3 expression, as performed in the present study, we expect to have captured the vast majority of DC. In support of this, similar proportions for main DC subsets were found in scRNA-seq (Flt3-enriched) and flow cytometry (Flt3-independent gating strategy employed for bulk RNA-seq of DC subsets). However, DC subsets expressing low levels of Flt3 (e.g. pDC) may still be missed by this enrichment strategy, as also discussed for scRNA-seq of Flt3-enriched cells in bovine lymph node (62).

Taken together, by enriching Flt3⁺ cells for scRNA-seq, we have zoomed into the heterogeneous compartment of porcine DC at unprecedented detail. Apart from discovering tDC as a major DC subset in porcine blood, we describe putative DC3 as *FLT3* expressing cells that show considerable transcriptional overlap with monocytes. Several open questions need to be addressed in future studies, including the functional role of these DC subsets across species, and the suitability of the pig as a model species for human tDC research.

Material and methods

Animals and isolation of PBMC

Blood was obtained from Swiss Large White pigs (Table 1), kept under specific-pathogen-free (SPF) conditions (63) at the animal facility of the IVI (Mittelhäusern, Switzerland), by puncturing the jugular vein. As anti-coagulant, citrate-based Alsever's solution (1.55 mM $C_6H_{12}O_6$; 408 mM $Na_3C_6H_5O_7$ ·2 H_2O ; 1.078 mM NaCl; 43 mM $C_6H_8O_7$, pH 6.2) was used.

For peripheral blood mononuclear cell (PBMC) isolation, blood was centrifuged at 1,000 x g for 20 min (room temperature; RT), the buffy coat was collected, diluted in PBS/EDTA (PBS; 1 mM EDTA) to a 1:1 ratio (RT) and layered onto Ficoll-paque (1.077 g/L, GE Healthcare) in Leucosep tubes (Greiner BioOne) for centrifugation at 800 x g for 25 min (RT). PBMC were collected and washed first once with cold PBS/EDTA at 350 x g for 10 min (4 °C, Ficoll-paque removal) and then once reducing the speed to 250 x g (platelet removal). Remaining, red blood cells were removed from the PBMC by incubation with cold lysis buffer (10 mM NaHCO₃; 1 mM EDTA; 0.15 M NH₄Cl, pH 7.25) for 10 min on ice, followed by two washes with cold PBS/EDTA at 250 x g for 10 min (4 °C).

Phenotyping of putative porcine tDC in blood by flow cytometry

The flow cytometry gating strategy used to identify mononuclear phagocyte (MP) subsets in pig blood was previously described by our laboratory (4), defining cDC1 as CD14⁻CD172a^{low}CADM1⁺ cells, cDC2 as CD14 CD172a CADM1 cells, pDC as CD14 CD172a+CADM1-CD4+ cells and monocytes as CD14+ cells. The same staining panel was used to gate on the newly identified DC subset as CD14⁻CD172a⁺CADM1⁻CD4⁻ cells in the present study. Briefly, a four-step four-color staining of PBMC was performed. Antibodies and porcine recombinant proteins used are listed in Table 2. Briefly, cells were first stained with the primary antibodies anti-CD172a (clone 74-22-15A) and anti-SynCAM (TSLC1/ CADM1, clone 3E1), followed by a second incubation with the corresponding secondary anti-mouse-IgG2b-AF647 and antichicken IgY biotin. A blocking step was then performed with ChromPure mouse IgG (Jackson Immunoresearch), and cells were finally incubated with the directly conjugated antibodies anti-CD14-FITC (clone MIL2) and anti-CD4-PerCP-Cy5.5 (clone 74-12-4), and with V500-conjugated streptavidin. Based on this staining, the phenotype of the new DC subset of interest was further characterized by analyzing the expression of additional cell surface markers, alongside corresponding FMO (Fluorescence minus one) controls. Flow cytometry acquisitions were performed on a FACS Canto II (BD Biosciences) equipped with three lasers (405, 488, and 633 nm) and a Cytek Aurora (Cytek Biosciences) equipped with four lasers (405, 488, 561, and 640 nm), software and were further analyzed with the Flowjo software (TreeStar, version 10.10.0).

Sorting and bulk RNA sequencing of putative porcine blood tDC

The newly identified DC subset was sorted from the blood of four pigs (12- to 24-month-old) for bulk RNA-seq analysis. First, a T-cell depletion of PBMC was performed using magnetic activated cell sorting with an anti-CD3 antibody (clone PPT3), anti-mouse IgG MicroBeads and LD columns (MACS MicroBead Technology,

TABLE 1 Animals used in each experiment.

Experiment	Number of pigs (Swiss Large White)	Age	Sex		
Bulk RNA-seq of sorted cDC1, cDC2, pDC and monocytes					
(From Auray et al., 2016)	n = 3	3–12 months	F		
Bulk RNA-seq of sorted pptDC					
	n = 4	12-24 months	F		
scRNA-seq of enriched DC					
	n = 3	16.5 months	F		

TABLE 2 List of antibodies and porcine recombinant proteins for phenotyping and FACS.

Experiment	Antigen or receptor ^a	Clone/Source of mAb	Detection/Source	
Phenotyping ¹ /	FACS for bulk RNA-seq ²			
Core	CD172a	74-22-15A/Vetmeduni Vienna, Austria	Anti-mouse IgG2b:AF647/Molecular Probes	
	CADM1*	3E1/MBL	Anti-chicken IgY:biotin/Jackson Immunoresearch + V500-coupled streptavidin/BD Horizon ¹ or + APC-AF750-coupled streptavidin/ Thermo Fisher ²	
	CD14	MIL2:FITC/AbD Serotec		
	CD4	74-12-4:PerCP-Cy5.5/BD Pharmingen		
Phenotypic markers	wC11R1/CD11b	MIL4/Serotec	Anti-mouse IgG1:RPE/SouthernBiotech	
	CD1.1	76-7-4/Vetmeduni Vienna, Austria	Anti-mouse IgG2a:RPE/SouthernBiotech	
	CD115/CSF1R	ROS8G11-1/Roslin Institute, University of Edinburgh, UK	Anti-mouse IgG2a:RPE/SouthernBiotech	
	CD163	2A10-11/INIA-CSIC, Madrid, Spain	Anti-mouse IgG1:RPE/SouthernBiotech	
	CD205	ZH9F7/CIAD, Hermosillo, Mexico	Anti-mouse IgG1:RPE/SouthernBiotech	
	CD303	102G7/Dendritics, Lyon France	Anti-mouse IgG1:RPE/SouthernBiotech	
	MHC-II/SLA-DQ	TH16B/VMRD	Anti-mouse IgG2a:RPE/SouthernBiotech	
	CD16	G7:RPE/AdB Serotec		
	CD135/Flt3 ^a	His-tagged porcine recombinant protein Flt3L/ In house	Anti-His: PE/Miltenyi Biotec	
	CD123/IL-3RA ^a	His-tagged porcine recombinant protein IL-3/ In house	Anti-His: RPE/Miltenyi Biotec	
T-cell depletion	CD3	PPT3-FyH2/University of Bristol, UK	Anti-mouse IgG:magnetic beads/Miltenyi Biotec	
DC enrichmen	t for scRNA-seq			
Core	CD172a	74-22-15A/Vetmeduni Vienna, Austria	Anti-mouse IgG2b:AF647/Molecular Probes	
	CD135/Flt3 ^a	His-tagged porcine recombinant protein Flt3L/ In house	Anti-His: PE/Miltenyi Biotec	
T-cell depletion	CD3	8E6-8C8/Kingfisher Biotech	Anti-mouse IgG2a:biotin + Magnetic beads:streptavidin/Miltenyi Biotec	

^{*} Anti-mouse CADM1 with pig cross reactivity.

Miltenyi Biotec). The same four-step four-color staining as described above was performed with the CD3-negative fraction, but V500-conjugated streptavidin was replaced by APC-AF750 streptavidin, and the DC subset of interest was sorted using fluorescence-activated cell sorting (FACS; FACSAria III; BD Biosciences). Finally, cells were resuspended in TRIzol (Life Technologies) and stored at -80 °C until later RNA extraction with the Nucleospin RNA kit (Macherey Nagel) as previously described (4). RNA quantification and quality assessment was performed with an Agilent 2100 Bioanalyzer (Agilent Technologies) and a Qubit 2.0 Fluorometer (Life Technologies). High-quality RNA (approximately 500 ng; RNA integrity number (RIN) > 8) was used to prepare non-directional paired-end mRNA

libraries with the TruSeq Sample Preparation Kit (v2, Illumina). The libraries were sequenced on the Illumina HiSeq2500 platform using 2 x 100 bp paired-end sequencing cycles, yielding between 26.5 and 30.1 million read pairs per sample. The Illumina BCL output files with base calls and qualities were converted into FASTQ file format and demultiplexed with the CASAVA software (v1.8.2). Raw bulk RNA-seq data for the cDC1, cDC2, pDC and monocytes (n = 3 pigs) were available from our previous work (4).

For analysis of bulk RNA-seq data, the following bioinformatics tools were used with their default parameters, unless specified otherwise. The quality of reads was assessed with fastQC v0.11.9 (https://www.bioinformatics.babraham.ac.uk/projects/fastqc/) and both low quality bases (Phred score < 30) and Illumina TruSeq2

adapters were trimmed with Trimmomatic v0.39 (64). The reads were then mapped to the pig reference genome (assembly Sscrofa 11.1) using STAR v2.7.10a (65). The duplicate reads were identified and removed using MarkDuplicates from the Picard command-line tools v2.25.1 (https://broadinstitute.github.io/picard/). The featureCounts program included in the SourceForge Subread package v2.0.3 (66) was used to count the number of reads overlapping with each gene identified in the Ensembl pig annotation release 11.1.111. In summary, (i) a minimum of 93.7% of reads were mapped to the genome among all samples, yielding between 29.6 and 57.2 million reads aligned per sample, (ii) between 14.2 and 35.4% of reads were identified as duplicates and (iii) 58.5-68.9% of reads were assigned to a gene, corresponding to a range of 16.3-33.0 million mapped reads.

The differential gene expression analyses were performed using the Bioconductor package DESeq2 v1.42.1 (67) in R v4.3.3 (68). Only genes with |log2FC| > 1 and adjusted p-value < 0.05 were selected as differentially expressed genes (DEGs). We performed pairwise comparisons of cell subsets as well as the comparison of each subset versus all others to define the MP subset-specific transcriptomic signatures (results are available as Data S1). Principal component analysis (PCA) was performed with normalized and vst-transformed counts of the 500 most variable genes across samples. Sample-sample correlation analysis was based on normalized gene expression data for each sample (counts()) using the Spearman correlation coefficient with hierarchical clustering based on Spearman distances.

Enrichment of DC by fluorescenceactivated cell sorting

To enrich DC for scRNA-seq analysis, a four-step protocol combining cell staining and T-cell depletion was performed on freshly isolated PBMC from three pigs in parallel. Antibodies and porcine recombinant proteins used are listed in Table 2. Briefly, 5 x 10⁸ PBMC were first stained with a His-tagged porcine recombinant protein Flt3L and the primary antibodies anti-CD172a (clone 74-22-15A) and anti-CD3 (clone 8E6-8C8), followed by a second incubation step with the corresponding secondary antibodies anti-His-PE, anti-mouse IgG2b AF647 and anti-mouse IgG2a biotin. Next, following incubation with Streptavidin MicroBeads (Miltenyi Biotec), CD3⁺ cells were depleted using LD columns (Miltenyi Biotec). Finally, total DC from the three pigs identified as Flt3⁺CD172a^{-/+} cells were sorted in parallel using one FACS Aria II and two FACS Aria III (all BD Bioscience) at the flow cytometry and cell sorting core facility at the University of Bern.

Single-cell RNA-seq (10x Genomics)

For scRNA-seq, DC isolated from the blood of three pigs (16.5-month-old) were analyzed with 10x Genomics. Gel beads-in-emulsion (GEM) generation and barcoding, reverse transcription, cDNA amplification and 3' gene expression library generation steps were all performed according to the Chromium Next GEM Single Cell 3'

Reagent Kits v3.1 (Dual Index) User Guide (10x Genomics CG000315, Rev E) with all stipulated 10x Genomics reagents. Generally, 9-11 µL of each cell suspension (1 500-1-900 cells/µL) and 32-35 µL of nucleasefree water were used for a targeted cell recovery of 10,000 cells. GEM generation was followed by a GEM-reverse transcription incubation, a clean-up step and 11 cycles of cDNA amplification. The resulting cDNA was evaluated for quantity and quality using a Thermo Fisher Scientific Qubit 4.0 fluorometer with the Qubit dsDNA HS Assay Kit (Thermo Fisher Scientific, Q32851) and an Advanced Analytical Fragment Analyzer System using a Fragment Analyzer NGS Fragment Kit (Agilent, DNF-473), respectively. Thereafter, 3' sc gene expression libraries were constructed using a sample index PCR step of 14 cycles. The generated cDNA libraries were tested for quantity and quality using fluorometry and capillary electrophoresis as described above. The cDNA libraries were pooled and sequenced with a loading concentration of 300 pM, asymmetric paired-end and dual indexed, on two shared Illumina NovaSeq 6000 sequencer using a NovaSeq 6000 S4 Reagent Kits v1.5 (200 cycles; Illumina, 20028313). The read set-up was as follows: read 1: 29 cycles, i7 index: 10 cycles, i5: 10 cycles and read 2: 91 cycles. The quality of the sequencing runs was assessed using Illumina Sequencing Analysis Viewer (v2.4.7, Illumina) and all base call files were demultiplexed and converted into FASTQ files using bcl2fastq conversion software (v2.20, Illumina). The mean reads per cell and number of cells obtained per sample ranged from 33-896 to 51-718 reads, and from 11-5311 to 14-221 cells, respectively All steps were performed at the Next Generation Sequencing Platform, University of Bern.

Analysis of porcine scRNA-seq data

Read alignment, quality control and filtering

The scRNA-seq FASTQ files were processed using Cell Ranger v7.1.0 (10x Genomics) (69) and reads were aligned to the pig reference genome (assembly Sscrofa 11.1). Bam files and filtered expression matrices were generated using the "cellranger_count" pipeline with default parameters, unless specified otherwise. Expression matrices were further analyzed in R v4.3.3 (68) using mainly Seurat v5.1.0 (70) and other R packages (list available in the GitHub page, see "Code availability" section). Quality-based scRNAseq data filtering was performed by excluding low-quality cells and dead cells (< 500 genes and > 10% of transcripts mapping to mitochondrial genes), non-expressed genes (genes expressed in < 5 cells across all samples) and cells identified with high probability as doublet by the scDblFinder package v1.16.0 (71) (doublet score threshold automatically determined). Percentages of mitochondrial and ribosomal protein gene expression in cells were calculated based on ND1, ND2, COX1, COX2, ATP8, ATP6, COX3, ND3, ND4L, ND4, ND5, ND6, CYTB genes and 61 RPS- and RPL- genes, respectively.

Normalization, dimensionality reduction, data integration and clustering

The three scRNA-seq samples loaded in a Seurat object (1 layer/sample) were independently processed for sctransform-based normalization, including steps of data scaling and highly variable

gene identification, and for linear dimensionality reduction using PCA. For further downstream analysis, the optimal number of 50 principal components (PCs) was identified by the elbowplot method. Cells were then scored for cell cycle phases based on their expression of S and G2M phase-associated genes listed in Seurat. Next, data integration of the three datasets was performed with Harmony v1.2.0 (72) on PCA cell embeddings and selecting the sample origin (batch effect correction) and the cell cycle phase as covariates. The resulting Harmony reduction was selected for identifying nearest neighbors, clustering the cells with the Leiden algorithm (method = "igraph", clustering resolution = 0.6), and performing non-linear dimensionality reduction using UMAP for cluster visualization.

Differential gene expression analysis

Counts in the RNA assay were log-normalized and scaled, and layers were joined. The DEGs in each cluster were identified with the *FindAllMarkers()* function and pairwise comparisons between selected clusters were performed with the *FindMarkers()* function. Only genes expressed in at least 20% of the cells in one of the clusters being compared, with |avg_log2FC| > 1 and adjusted p-value < 0.05 were selected as DEGs. In addition, DEGs from pairwise comparisons were filtered according to an expression in at least 20% of the cells in one of the clusters being compared and 80% of the cells in the other one(s).

Cluster correlation analysis

Cluster-cluster correlation values were calculated based on averaged log-normalized gene expression data for each cluster using the Spearman correlation coefficient.

Gene set enrichment analysis

Gene set enrichment analyses (GSEA) were performed with the AUCell package v1.24.0 (73) as previously described by Herrera-Uribe et al. (74). Briefly, the expression of the specific enriched gene set in each sorted porcine blood MP subset analyzed by bulk RNAseq (as described in preceding methods) was evaluated within cells of the scRNA-seq dataset, as follows: Ranking of gene expression from raw gene counts and calculation of area under the curve (AUC) scores from the top 5, 10, 15, 25, 50 and 100% of expressed genes in a cell and the gene sets. AUC scores are proportional to the percentage of genes from a gene set found in the top expressed genes for a cell defined at different levels. Next, AUC scores and UMAP coordinates of each cell were overlayed for UMAP visualization, with manual determination of a threshold value for each gene set based on AUC score distributions. Heatmap representation was based on averaged scaled AUC scores calculated for each cluster, following scaling of individual cell AUC scores relative to other cells within a single gene set comparison (rows) but not between gene sets (columns).

For species comparison, GSEA were performed with DC subset gene signatures from three sources: (i) a published scRNA-seq study (SMARTSeq2) of human blood DC (19), (ii) a published bulk and scRNA-seq study of murine spleen DC (10x Genomics) (24), and (iii) results from re-analysis of a recently published scRNA-seq

dataset (10x Genomics) of human blood DC (50). The pig orthologs of human and mouse genes were identified with BioMart (Ensembl) and selected according to the highest percentage of identity to the target pig gene. Human and mouse genes without pig orthologs were removed. The resulting pig-converted- human and murine gene signatures are provided as Data S2. GSEA were performed as described above, calculating the AUC scores from the top 25% of expressed genes in a cell and the gene sets and represented as heatmaps.

Machine-learning-based cell scoring

The classification score for the different cell clusters was created with the scikit-learn python module (75) as previously described by Mayère et al. (76). An ElasticNet model with one versus all approach was trained using the *ElasticNet()* function (alpha = 0.05, tol = 0.01) on a random subsample of 450 cells per cluster in order to avoid gene weighting bias due to overrepresentation of some clusters. The ElasticNet approach uses a linear regression with combined L1 (Lasso) and L2 (Ridge) priors as regularizer, allowing a robust selection of relevant genes defining the cells of interest (77, 78).

Cluster subsetting

Subsetting was performed using the Seurat's *subset()* function. Non-expressed genes in the new datasets were removed with *DietSeurat()* and data were split according to the sample of origin using the *split()* function (1 layer/sample). Data were then reprocessed for normalization, dimensional reduction, data integration and clustering (method = "igraph") as described above. Counts in the RNA assay were log-normalized and scaled, and layers were joined.

Trajectory inference analysis

The trajectory inference analysis of the subsetted dataset was performed with the Scorpius package v1.0.9 (79). Cells were ordered according to the inferred linear trajectory using the <code>infer_trajectory</code> () function and the importance of a gene and its expression with respect to the modelled dynamic process was assessed with the <code>gene_importances()</code> function. Next, the top 50 important genes were assigned into modules according to their expression patterns across the inferred trajectory with the <code>extract_modules()</code> function, using the normalized expression values scaled from 0 to 1 with the <code>scale_quantile()</code> function.

Analysis of published scRNA-seq data (human DC)

We analyzed the scRNA-seq dataset of human blood DC recently generated by Lubin et al. (50) (approximately 3,000 cells). DC were sorted by flow cytometry and subjected to 10x Genomics scRNA-seq. Processed data from the cellranger pipeline (barcode, feature and matrix files), available under the sample number GSM8499782 in the National Center for Biotechnology Information Gene Expression Omnibus database, were analyzed

with the Seurat pipeline as described above for the porcine data (quality-based data filtering, sctransform-based normalization and linear dimensional reduction using PCA). The PCA reduction was selected for identifying nearest neighbors, clustering the cells with the Leiden algorithm (method = "igraph", clustering resolution = 0.8), and performing non-linear dimensional reduction using UMAP for cluster visualization. Next, the differential gene expression analysis was performed as for the porcine data, using FindAllMarkers() to identify the DEGs in each cluster.

Identification and replacement of gene identifiers

Pig gene Ensembl stable identifiers (IDs) without available gene name/symbol in the pig genome annotation file were replaced in text and figures by NCBI gene (formerly Entrezgene) accession or UniProtKB Gene Name symbol if available in the corresponding databases using the BioMart data mining tool from Ensembl (https://www.ensembl.org/biomart/martview). A list of replaced Ensembl IDs is included in Data S1. The human gene names HLA-DRA and HLA-DOB found in the pig genome annotation were replaced by SLA-DRA and SLA-DOB respectively, the gene names of their porcine orthologs. While IL3RA is not currently annotated in the Ensembl pig genome, it is available in the NCBI reference. Thus, the porcine genomic sequence for the gene encoding IL3RA (ENSSSCG00000055271) was identified by aligning the IL3RA gene sequence from NCBI (gene identifier: 102166116) to the Ensembl pig genome (Sscrofa release 11.1.111) using the Ensembl BLAT (100% sequence identity). The sequence of the IL3RA transcript ENSSSCT00000092699, product of the ENSSSCG00000055271 gene (IL3RA), was utilized to visualize the read distribution across its corresponding genomic location (AEMK02000569.1: 775,837-784,610) for each sorted MP subset, using Integrative Genomics Viewer (IGV) software.

Preparation of figures

Figures were prepared using FlowJoTM v10.10.0 (BD Life Sciences) (80), R v4.3.3 (68), Rstudio v2024.04.1 (81), Inkscape v1.3.2 (https://www.inkscape.org), Integrative Genomics Viewer (IGV) v2.17.4 (82) softwares. FACS scheme was created using Servier Medical Art, by Servier (http://smart.servier.com).

Bulk RNA-seq data was represented as PCA and heatmaps using the ggplot2 v3.5.1 (83) and ComplexHeatmap v2.18.0 (84) R packages, respectively. Heatmaps were prepared following log10 transformation of normalized counts. Prior to log10 transformation, a pseudocount of 1 was added to the values to avoid zeros.

Visualization of scRNA-seq data was based on feature plots, dot plots, violin plots, bar plots, scatter plots and heatmaps using the Seurat v5.1.0 (70), scCustomize v2.1.2 (85), ggplot2 v3.5.1 (83) and

ComplexHeatmap v2.18.0 (84) R packages. Heatmaps were generated with scaled and centered data (Seurat *ScaleData() function*). For improved contrast in feature plots, feature-specific contrast levels were calculated based on quantiles (q10, q90) of nonzero expression.

The cell classification scoring based on a machine learning model was visualized by scatter plots using the scikit-learn python module (75).

The trajectory inference analysis was represented as UMAP plot and heatmap using the Scorpius R package v1.0.9 (79).

Code availability

Scripts used for read alignment to the pig reference genome and the bulk and scRNA-seq data analyses are available in the following GitHub public repository: https://github.com/IVI-Immunology/Porcine_blood_DC_scRNA-seq.

Data availability statement

Raw sequencing data from bulk RNA-seq of pig blood cDC1, cDC2, pDC and monocytes are available in the European Nucleotide Archive (ENA) (http://www.ebi.ac.uk/ena) under the accession number PRJEB15381. Raw sequencing data from bulk RNA-seq of porcine blood tDC and from scRNA-seq is available in ENA under the accession number PRJEB101131.

Ethics statement

Blood sampling of pigs was performed in compliance with the Swiss animal protection law (TSchG SR 455; TSchV SR 455.1; TVV SR 455.163). The procedures were reviewed by the committee on animal experiments of the canton of Bern, Switzerland, and approved by the cantonal veterinary authority (Amt für Landwirtschaft und Natur LANAT, Veterinärdienst VeD, Bern, Switzerland) under the licence numbers BE88/14 and BE127/2020. The study was conducted in accordance with the local legislation and institutional requirements.

Author contributions

AB: Formal analysis, Investigation, Methodology, Visualization, Writing – original draft, Writing – review & editing. GA: Formal analysis, Investigation, Writing – review & editing. FB: Methodology, Supervision, Writing – review & editing. MB: Methodology, Writing – review & editing. AH: Formal analysis, Methodology, Writing – review & editing, Investigation. AS: Conceptualization, Project administration, Resources, Supervision, Validation, Writing – review & editing, Funding acquisition. ST: Conceptualization, Investigation,

Methodology, Project administration, Supervision, Validation, Writing – original draft, Writing – review & editing, Funding acquisition.

Funding

The author(s) declare financial support was received for the research and/or publication of this article. Part of this work has received funding from the Swiss State Secretariat for Education, Research and Innovation (SERI) Nr. 24.00582 under the umbrella of the European Union Innovative Health Initiative (EU-IHI) Joint Undertaking (JU), as part of the NHPig project 101165643.

Acknowledgments

We thank Sylvie Python and Caroline Lehmann (IVI, Bern, Switzerland) for their support in the laboratory, animal caretakers at IVI for blood sampling, Stefan Müller (FCCS, University of Bern, Switzerland) for cell sorting, Pamela Nicholson (NGS Platform, University of Bern, Switzerland) for single-cell RNA sequencing, and the Interfaculty Bioinformatics Unit (IBU, University of Bern, Switzerland) for access to their compute cluster.

Conflict of interest

The authors declare that the research was conducted in the absence of any commercial or financial relationships that could be construed as a potential conflict of interest.

The author(s) declared that they were an editorial board member of Frontiers, at the time of submission. This had no impact on the peer review process and the final decision.

Generative AI statement

The author(s) declare that no Generative AI was used in the creation of this manuscript.

Any alternative text (alt text) provided alongside figures in this article has been generated by Frontiers with the support of artificial intelligence and reasonable efforts have been made to ensure accuracy, including review by the authors wherever possible. If you identify any issues, please contact us.

Publisher's note

All claims expressed in this article are solely those of the authors and do not necessarily represent those of their affiliated organizations, or those of the publisher, the editors and the reviewers. Any product that may be evaluated in this article, or claim that may be made by its manufacturer, is not guaranteed or endorsed by the publisher.

Supplementary material

The Supplementary Material for this article can be found online at: https://www.frontiersin.org/articles/10.3389/fimmu.2025.1639553/full#supplementary-material

References

- 1. Cabeza-Cabrerizo M, Cardoso A, Minutti CM, Pereira Da Costa M, Reis E Sousa C. Dendritic cells revisited. *Annu Rev Immunol.* (2021) 39:131–66. doi: 10.1146/annurev-immunol-061020-053707
- 2. Collin M, Bigley V. Human dendritic cell subsets: an update. *Immunology.* (2018) 154:3–20. doi: 10.1111/imm.12888
- 3. Zhang S, Audiger C, Chopin M, Nutt SL. Transcriptional regulation of dendritic cell development and function. *Front Immunol.* (2023) 14:1182553. doi: 10.3389/fimmu.2023.1182553
- 4. Auray G, Keller I, Python S, Gerber M, Bruggmann R, Ruggli N, et al. Characterization and transcriptomic analysis of porcine blood conventional and plasmacytoid dendritic cells reveals striking species-specific differences. *J Immunol.* (2016) 197:4791–806. doi: 10.4049/jimmunol.1600672
- 5. Auray G, Talker SC, Keller I, Python S, Gerber M, Liniger M, et al. High-Resolution Profiling of Innate Immune Responses by Porcine Dendritic Cell Subsets *in vitro* and in *vivo*. *Front Immunol*. (2020) 11:1429. doi: 10.3389/fimmu.2020.01429
- 6. Summerfield A, Auray G, Ricklin M. Comparative dendritic cell biology of veterinary mammals. *Annu Rev Anim Biosci.* (2015) 3:533–57. doi: 10.1146/annurevanimal-022114-111009
- 7. Talker SC, Baumann A, Barut GT, Keller I, Bruggmann R, Summerfield A. Precise delineation and transcriptional characterization of bovine blood dendritic-cell and monocyte subsets. *Front Immunol.* (2018) 9:2505. doi: 10.3389/fimmu.2018.02505
- 8. Barut GT, Lischer HEL, Bruggmann R, Summerfield A, Talker SC. Transcriptomic profiling of bovine blood dendritic cells and monocytes following TLR stimulation. *Eur J Immunol.* (2020) 50:1691–711. doi: 10.1002/eji.202048643
- 9. Ziegler A, Marti E, Summerfield A, Baumann A. Identification and characterization of equine blood plasmacytoid dendritic cells. *Dev Comp Immunol.* (2016) 65:352–7. doi: 10.1016/j.dci.2016.08.005

- 10. Baillou A, Tomal F, Chaumeil T, Barc C, Levern Y, Sausset A, et al. Characterization of intestinal mononuclear phagocyte subsets in young ruminants at homeostasis and during Cryptosporidium parvum infection. *Front Immunol.* (2024) 15:1379798. doi: 10.3389/fimmu.2024.1379798
- 11. Chen B, Zhu L, Yang S, Su W. Unraveling the heterogeneity and ontogeny of dendritic cells using single-cell RNA sequencing. *Front Immunol.* (2021) 12:711329. doi: 10.3389/fimmu.2021.711329
- 12. Dutertre CA, Becht E, Irac SE, Khalilnezhad A, Narang V, Khalilnezhad S, et al. Single-cell analysis of human mononuclear phagocytes reveals subset-defining markers and identifies circulating inflammatory dendritic cells. *Immunity*. (2019) 51:573–589.e8. doi: 10.1016/j.immuni.2019.08.008
- 13. Minutti CM, Piot C, Pereira Da Costa M, Chakravarty P, Rogers N, Huerga Encabo H, et al. Distinct ontogenetic lineages dictate cDC2 heterogeneity. *Nat Immunol.* (2024) 25:448–61. doi: 10.1038/s41590-024-01745-9
- 14. Cytlak U, Resteu A, Pagan S, Green K, Milne P, Maisuria S, et al. Differential IRF8 transcription factor requirement defines two pathways of dendritic cell development in humans. *Immunity*. (2020) 53:353–370.e8. doi: 10.1016/j.immuni.2020.07.003
- 15. Rodrigues PF, Trsan T, Cvijetic G, Khantakova D, Panda SK, Liu Z, et al. Progenitors of distinct lineages shape the diversity of mature type 2 conventional dendritic cells. *Immunity*. (2024) 57:1567–1585.e5. doi: 10.1016/j.immuni.2024.05.007
- 16. León B. Type 2 conventional dendritic cell functional heterogeneity: ontogenically committed or environmentally plastic? *Trends Immunol.* (2025) 46 (2):104–20. doi: 10.1016/j.it.2024.12.005
- 17. Bourdely P, Anselmi G, Vaivode K, Ramos RN, Missolo-Koussou Y, Hidalgo S, et al. Transcriptional and functional analysis of CD1c+ Human dendritic cells identifies a CD163+ Subset priming CD8+CD103+ T cells. *Immunity.* (2020) 53:335–352.e8. doi: 10.1016/j.immuni.2020.06.002

- 18. Liu Z, Wang H, Li Z, Dress RJ, Zhu Y, Zhang S, et al. Dendritic cell type 3 arises from Ly6C+ monocyte-dendritic cell progenitors. *Immunity*. (2023) 56:1761–1777.e6. doi: 10.1016/j.immuni.2023.07.001
- 19. Villani AC, Satija R, Reynolds G, Sarkizova S, Shekhar K, Fletcher J, et al. Single-cell RNA-seq reveals new types of human blood dendritic cells, monocytes, and progenitors. *Science*. (2017) 356:eaah4573. doi: 10.1126/science.aah4573
- 20. Rodrigues PF, Alberti-Servera L, Eremin A, Grajales-Reyes GE, Ivanek R, Tussiwand R. Distinct progenitor lineages contribute to the heterogeneity of plasmacytoid dendritic cells. *Nat Immunol.* (2018) 19:711–22. doi: 10.1038/s41590-018-0136-9
- 21. Arroyo Hornero R, Idoyaga J. Plasmacytoid dendritic cells: A dendritic cell in disguise. *Mol Immunol.* (2023) 159:38–45. doi: 10.1016/j.molimm.2023.05.007
- 22. Leylek R, Alcántara-Hernández M, Lanzar Z, Lüdtke A, Perez OA, Reizis B, et al. Integrated cross-species analysis identifies a conserved transitional dendritic cell population. *Cell Rep.* (2019) 29:3736–3750.e8. doi: 10.1016/j.celrep.2019.11.042
- 23. Matsui T, Connolly JE, Michnevitz M, Chaussabel D, Yu CI, Glaser C, et al. CD2 distinguishes two subsets of human plasmacytoid dendritic cells with distinct phenotype and functions. *J Immunol*. (2009) 182:6815–23. doi: 10.4049/immunol.0802008
- 24. Sulczewski FB, Maqueda-Alfaro RA, Alcántara-Hernández M, Perez OA, Saravanan S, Yun TJ, et al. Transitional dendritic cells are distinct from conventional DC2 precursors and mediate proinflammatory antiviral responses. *Nat Immunol.* (2023) 24:1265–80. doi: 10.1038/s41590-023-01545-7
- 25. Salvermoser J, Van Blijswijk J, Papaioannou NE, Rambichler S, Pasztoi M, Pakalniškytė D, et al. Clec9a-mediated ablation of conventional dendritic cells suggests a lymphoid path to generating dendritic cells *in vivo. Front Immunol.* (2018) 9:699. doi: 10.3389/fimmu.2018.00699
- 26. Rodrigues PF, Kouklas A, Cvijetic G, Bouladoux N, Mitrovic M, Desai JV, et al. pDC-like cells are pre-DC2 and require KLF4 to control homeostatic CD4 T cells. *Sci Immunol.* (2023) 8:eadd4132. doi: 10.1126/sciimmunol.add4132
- 27. Domínguez J. Workshop studies on monoclonal antibodies in the myeloid panel with CD11 specificity. *Veterinary Immunol Immunopathology*. (2001) 80:111–9. doi: 10.1016/S0165-2427(01)00286-0
- 28. Nutt SL, Chopin M. Transcriptional networks driving dendritic cell differentiation and function. *Immunity*. (2020) 52:942-56. doi: 10.1016/j.immuni.2020.05.005
- 29. Vu Manh TP, Elhmouzi-Younes J, Urien C, Ruscanu S, Jouneau L, Bourge M, et al. Defining mononuclear phagocyte subset homology across several distant warm-blooded vertebrates through comparative transcriptomics. *Front Immunol.* (2015) 6:299/abstract. doi: 10.3389/fimmu.2015.00299/abstract
- 30. Leylek R, Alcántara-Hernández M, Granja JM, Chavez M, Perez K, Diaz OR, et al. Chromatin landscape underpinning human dendritic cell heterogeneity. *Cell Rep.* (2020) 32:108180. doi: 10.1016/j.celrep.2020.108180
- 31. Valente M, Collinet N, Vu Manh TP, Popoff D, Rahmani K, Naciri K, et al. Novel mouse models based on intersectional genetics to identify and characterize plasmacytoid dendritic cells. *Nat Immunol.* (2023) 24:714–28. doi: 10.1038/s41590-023-01454-9
- 32. Grajkowska LT, Ceribelli M, Lau CM, Warren ME, Tiniakou I, Nakandakari Higa S, et al. Isoform-specific expression and feedback regulation of E protein TCF4 control dendritic cell lineage specification. *Immunity*. (2017) 46:65–77. doi: 10.1016/j.immuni.2016.11.006
- 33. Doulatov S, Notta F, Rice KL, Howell L, Zelent A, Licht JD, et al. PLZF is a regulator of homeostatic and cytokine-induced myeloid development. *Genes Dev.* (2009) 23:2076–87. doi: 10.1101/gad.1788109
- 34. Geijtenbeek TBH, Gringhuis SI. Signalling through C-type lectin receptors: shaping immune responses. *Nat Rev Immunol.* (2009) 9:465–79. doi: 10.1038/nri2569
- 35. Scur M, Parsons BD, Dey S, Makrigiannis AP. The diverse roles of C-type lectin-like receptors in immunity. *Front Immunol.* (2023) 14:1126043. doi: 10.3389/fimmu.2023.1126043
- 36. Drouin M, Saenz J, Chiffoleau E. C-type lectin-like receptors: head or tail in cell death immunity. *Front Immunol.* (2020) 11:251. doi: 10.3389/fimmu.2020.00251
- 37. Lee HK, Mattei LM, Steinberg BE, Alberts P, Lee YH, Chervonsky A, et al. *In vivo* requirement for atg5 in antigen presentation by dendritic cells. *Immunity*. (2010) 32:227–39. doi: 10.1016/j.immuni.2009.12.006
- 38. Lei L, Bandola-Simon J, Roche PA. Ubiquitin-conjugating enzyme E2 D1 (Ube2D1) mediates lysine-independent ubiquitination of the E3 ubiquitin ligase March-I. *J Biol Chem.* (2018) 293:3904–12. doi: 10.1074/jbc.RA117.001322
- 39. Jancic C, Savina A, Wasmeier C, Tolmachova T, El-Benna J, Dang PMC, et al. Rab27a regulates phagosomal pH and NADPH oxidase recruitment to dendritic cell phagosomes. *Nat Cell Biol.* (2007) 9:367–78. doi: 10.1038/ncb1552
- 40. Harden JL, Egilmez NK. Indoleamine 2,3-dioxygenase and dendritic cell tolerogenicity. *Immunol Investigations*. (2012) 41:738-64. doi: 10.3109/08820139.2012.676122
- 41. Romagnani S. IL4I1: Key immunoregulator at a crossroads of divergent T-cell functions. Eur J Immunol. (2016) 46:2302–5. doi: 10.1002/eji.201646617

- 42. Gliddon DR, Howard CJ. CD26 is expressed on a restricted subpopulation of dendritic cells in *vivo*. Eur J Immunol. (2002) 32:1472. doi: 10.1002/1521-4141(200205) 32:5<1472::AID-IMMU1472>3.0.CO;2-Q
- 43. Zhou X, Khan S, Huang D, Li L. V-Set and immunoglobulin domain containing (VSIG) proteins as emerging immune checkpoint targets for cancer immunotherapy. *Front Immunol.* (2022) 13:938470. doi: 10.3389/fimmu.2022.938470
- 44. Kotwica-Mojzych K, Jodłowska-Jędrych B, Mojzych M. CD200:CD200R interactions and their importance in immunoregulation. *IJMS*. (2021) 22:1602. doi: 10.3390/ijms22041602
- 45. Reeh H, Rudolph N, Billing U, Christen H, Streif S, Bullinger E, et al. Response to IL-6 trans- and IL-6 classic signalling is determined by the ratio of the IL-6 receptor α to gp130 expression: fusing experimental insights and dynamic modelling. *Cell Commun Signal.* (2019) 17:46. doi: 10.1186/s12964-019-0356-0
- 46. Bachem A, Güttler S, Hartung E, Ebstein F, Schaefer M, Tannert A, et al. Superior antigen cross-presentation and XCR1 expression define human CD11c +CD141+ cells as homologues of mouse CD8+ dendritic cells. *J Exp Med.* (2010) 207:1273–81. doi: 10.1084/jem.20100348
- 47. Dorner BG, Dorner MB, Zhou X, Opitz C, Mora A, Güttler S, et al. Selective expression of the chemokine receptor XCR1 on cross-presenting dendritic cells determines cooperation with CD8+ T cells. *Immunity*. (2009) 31:823–33. doi: 10.1016/j.immuni.2009.08.027
- 48. Hong W, Yang B, He Q, Wang J, Weng Q. New insights of CCR7 signaling in dendritic cell migration and inflammatory diseases. *Front Pharmacol.* (2022) 13:841687. doi: 10.3389/fphar.2022.841687
- 49. Cordero H. Chemokine receptors in primary and secondary lymphoid tissues. *Int Rev Cell Mol Biol.* (2024), 1–19. doi: 10.1016/bs.ircmb.2023.11.003
- 50. Lubin R, Patel AA, Mackerodt J, Zhang Y, Gvili R, Mulder K, et al. The lifespan and kinetics of human dendritic cell subsets and their precursors in health and inflammation. *J Exp Med.* (2024) 221:e20220867. doi: 10.1084/jem.20220867
- 51. Sasaki I, Hoshino K, Sugiyama T, Yamazaki C, Yano T, Iizuka A, et al. Spi-B is critical for plasmacytoid dendritic cell function and development. *Blood.* (2012) 120:4733–43. doi: 10.1182/blood-2012-06-436527
- 52. Alcántara-Hernández M, Leylek R, Wagar LE, Engleman EG, Keler T, Marinkovich MP, et al. High-dimensional phenotypic mapping of human dendritic cells reveals interindividual variation and tissue specialization. *Immunity.* (2017) 47:1037–1050.e6. doi: 10.1016/j.immuni.2017.11.001
- 53. See P, Dutertre CA, Chen J, Günther P, McGovern N, Irac SE, et al. Mapping the human DC lineage through the integration of high-dimensional techniques. *Science*. (2017) 356:eaag3009. doi: 10.1126/science.aag3009
- 54. Luber CA, Cox J, Lauterbach H, Fancke B, Selbach M, Tschopp J, et al. Quantitative proteomics reveals subset-specific viral recognition in dendritic cells. *Immunity.* (2010) 32:279–89. doi: 10.1016/j.immuni.2010.01.013
- 55. Yamazaki C, Miyamoto R, Hoshino K, Fukuda Y, Sasaki I, Saito M, et al. Conservation of a chemokine system, XCR1 and its ligand, XCL1, between human and mice. *Biochem Biophys Res Commun.* (2010) 397:756–61. doi: 10.1016/j.bbrc.2010.06.029
- 56. Talker SC, Barut GT, Lischer HEL, Rufener R, Von Münchow L, Bruggmann R, et al. Monocyte biology conserved across species: Functional insights from cattle. *Front Immunol.* (2022) 13:889175. doi: 10.3389/fimmu.2022.889175
- 57. Busch R, Neese RA, Awada M, Hayes GM, Hellerstein MK. Measurement of cell proliferation by heavy water labeling. *Nat Protoc.* (2007) 2:3045–57. doi: 10.1038/nprot.2007.420
- 58. Patel AA, Zhang Y, Fullerton JN, Boelen L, Rongvaux A, Maini AA, et al. The fate and lifespan of human monocyte subsets in steady state and systemic inflammation. *J Exp Med.* (2017) 214:1913–23. doi: 10.1084/jem.20170355
- 59. Esashi E, Wang YH, Perng O, Qin XF, Liu YJ, Watowich SS. The signal transducer STAT5 inhibits plasmacytoid dendritic cell development by suppressing transcription factor IRF8. *Immunity*. (2008) 28:509–20. doi: 10.1016/j.immuni.2008.02.013
- 60. Edwards JC, Everett HE, Pedrera M, Mokhtar H, Marchi E, Soldevila F, et al. CD1– and CD1+ porcine blood dendritic cells are enriched for the orthologues of the two major mammalian conventional subsets. *Sci Rep.* (2017) 7:40942. doi: 10.1038/srep40942
- 61. Tussiwand R, Rodrigues PF. Where's Waldo: Identifying DCs within Mononuclear Phagocytes during Inflammation. *Immunity*. (2020) 52:892-4. doi: 10.1016/j.immuni.2020.05.006
- 62. Barut GT, Kreuzer M, Bruggmann R, Summerfield A, Talker SC. Single-cell transcriptomics reveals striking heterogeneity and functional organization of dendritic and monocytic cells in the bovine mesenteric lymph node. *Front Immunol.* (2023) 13:1099357. doi: 10.3389/fimmu.2022.1099357
- 63. Radulovic E, Mehinagic K, Wüthrich T, Hilty M, Posthaus H, Summerfield A, et al. The baseline immunological and hygienic status of pigs impact disease severity of African swine fever. *PloS Pathog.* (2022) 18:e1010522. doi: 10.1371/journal.ppat.1010522
- $64.\ Bolger\ AM,\ Lohse\ M,\ Usadel\ B.\ Trimmomatic: a flexible trimmer for Illumina sequence data.$ Bioinformatics. (2014) 30:2114–20. doi: 10.1093/bioinformatics/btu170

- 65. Dobin A, Davis CA, Schlesinger F, Drenkow J, Zaleski C, Jha S, et al. STAR: ultrafast universal RNA-seq aligner. *Bioinformatics*. (2013) 29:15–21. doi: 10.1093/bioinformatics/bts635
- 66. Liao Y, Smyth GK, Shi W. featureCounts: an efficient general purpose program for assigning sequence reads to genomic features. *Bioinformatics*. (2014) 30:923–30. doi: 10.1093/bioinformatics/btt656
- 67. Love MI, Huber W, Anders S. Moderated estimation of fold change and dispersion for RNA-seq data with DESeq2. *Genome Biol.* (2014) 15:550. doi: 10.1186/s13059-014-0550-8
- 68. R Core Team. R: A language and environment for statistical computing (2023). Vienna, Austria: R Foundation for Statistical Computing. Available online at: https://www.R-project.org/ (Accessed October 21, 2025).
- 69. Zheng GXY, Terry JM, Belgrader P, Ryvkin P, Bent ZW, Wilson R, et al. Massively parallel digital transcriptional profiling of single cells. *Nat Commun.* (2017) 8:14049. doi: 10.1038/ncomms14049
- 70. Hao Y, Stuart T, Kowalski MH, Choudhary S, Hoffman P, Hartman A, et al. Dictionary learning for integrative, multimodal and scalable single-cell analysis. *Nat Biotechnol.* (2023) 42(3):293–304. doi: 10.1038/s41587-023-01767-y
- 71. Germain PL, Lun A, Garcia Meixide C, Macnair W, Robinson MD. Doublet identification in single-cell sequencing data using scDblFinder. F1000Res. (2022) 10:979. doi: 10.12688/f1000research.73600.2
- 72. Korsunsky I, Fan J, Slowikowski K, Zhang F, Wei K, Baglaenko Y, et al. Fast, sensitive, and accurate integration of single cell data with Harmony. *Nat Methods*. (2018) 16(12):1289–96. doi: 10.1101/461954
- 73. Aibar S, González-Blas CB, Moerman T, Huynh-Thu VA, Imrichova H, Hulselmans G, et al. SCENIC: single-cell regulatory network inference and clustering. *Nat Methods.* (2017) 14:1083–6. doi: 10.1038/nmeth.4463
- 74. Herrera-Uribe J, Wiarda JE, Sivasankaran SK, Daharsh L, Liu H, Byrne KA, et al. Reference transcriptomes of porcine peripheral immune cells created through bulk and

- single-cell RNA sequencing. Front Genet. (2021) 12:689406. doi: 10.3389/fgene.2021.689406
- 75. Pedregosa F, Varoquaux G, Gramfort A, Michel V, Thirion B, Grisel O, et al. Scikit-learn: machine learning in python. *J Mach Learn Res.* (2011) 12:2825–30. doi: 10.5555/1953048.2078195
- 76. Mayère C, Regard V, Perea-Gomez A, Bunce C, Neirijnck Y, Djari C, et al. Origin, specification and differentiation of a rare supporting-like lineage in the developing mouse gonad. *Sci Adv.* (2022) 8:eabm0972. doi: 10.1126/sciadv.abm0972
- 77. Zou H, Hastie T. Regularization and variable selection via the elastic net. J R Stat Soc Ser B: Stat Methodology. (2005) 67:301–20. doi: 10.1111/j.1467-9868.2005.00503.x
- 78. Torang A, Gupta P, Klinke DJ. An elastic-net logistic regression approach to generate classifiers and gene signatures for types of immune cells and T helper cell subsets. *BMC Bioinf.* (2019) 20:433. doi: 10.1186/s12859-019-2994-z
- 79. Cannoodt R, Saelens W, Sichien D, Tavernier S, Janssens S, Guilliams M, et al. SCORPIUS improves trajectory inference and identifies novel modules in dendritic cell development. *bioRxiv* (2016). doi: 10.1101/079509
- 80. FlowJo™ Software (for Windows). Flow Cytometry Analysis. Ashland, OR: Becton, Dickinson and Company (2023).
- 81. RStudio Team. RStudio: Integrated Development Environment for R (2020). Boston, MA: RStudio, PBC. Available online at: http://www.rstudio.com/ (Accessed October 21, 2025).
- 82. Robinson JT, Thorvaldsdóttir H, Winckler W, Guttman M, Lander ES, Getz G, et al. Integrative genomics viewer. *Nat Biotechnol.* (2011) 29:24–6. doi: 10.1038/nbt.1754
- 83. Wickham H. ggplot2: elegant graphics for data analysis. 2nd ed. Switzerland: Springer (2016). p. 260.
- 84. Gu Z. Complex heatmap visualization. iMeta. (2022) 1:e43. doi: 10.1002/imt2.43
- 85. Marsh S, Salmon M, Hoffman P. samuel-marsh/scCustomize: version 2.1.2. Zenodo. (2024). doi: 10.5281/zenodo.5706430